JOURNAL OF LOW DIMENSIONAL SYSTEMS

Physics, Chemistry and Biology of Low Dimensional Systems
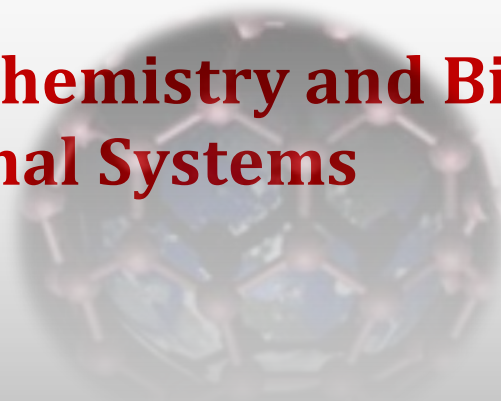
Aims and scope

The *Journal of Low Dimensional Systems* is co-edited by Baku State University.

It publishes papers and review articles on the fundamental and applied aspects of physics, chemistry and biology. General areas of interest are the electronic, spectroscopic and structural properties of low dimensional systems, including perfect and defect lattices, surfaces, two-dimensional electron systems, interfaces, thin films and multilayers, amorphous materials, micro- and nanostructures, and layered structures. Papers dealing with biomaterials for medical purposes are accepted.

Typical examples include the preparation and structural characterization of novel and advanced low dimensional materials, especially in relation to the measurement and interpretation of their electrical, magnetic, optical, thermal and mechanical properties, phase transitions, electronic structure and defect properties, and the application of appropriate experimental and theoretical techniques in these studies. Articles are encouraged in all the above areas, but especially those which emphasize fundamental aspects of materials science.

Address:

Az1148, Z.Khalilov str. 23,
Baku State University, BSU publication, Baku, Azerbaijan

E-mail: journal_lds@bsu.az

Table of Contents

SYNTHESIS AND STUDY OF THE ANTIMICROBIAL ACTIVITY OF (E) -1- (2,2-DICHLORO-1-PHENYLVINYL) -2-PHENYLDIAZENE

A.M. Maharramov, U.F.Askerova , N.E. Akhmedova,
S.Kh. Mukhtarova, Kh.A.Garazadeh, N.G. Shikhaliev

Baku State University, Z.Khalilov 23 Str., Baku, Azerbaijan
E-mail: namiqst@gmail.com

The phenylhydrazones of various benzaldehyde derivatives have been synthesized and, based on them has been carried out a catalytic olefination reaction with CCl4. The structure of synthesized dichlorodiazobutadienes was determined by X-ray diffraction and NMR methods. The presence of intermolecular non-covalent halogen-halogen (Cl ··· Cl) bonds was established. The antimicrobial activity of synthesized (E) -1- (2,2-dichloro-1-phenylvinyl) -2-phenyldiazene has been investigated and found to exert a suppressive effect on bacteria such as St. Aureus, Ps. Aeruginoza, E. coli, Cand. Albicans.

Keywords: Synthesis, phenylhydrazone, non-covalent bonds, antimicrobial.

1. INTRODUCTION

The modern approach to the synthesis of new organic compounds has already reached a new level. To this day, organic chemists synthesize new compounds not for the sake of novelty of structure, and etc., but carry out a more thoughtful synthesis, using the data and knowledge accumulated to the present day. Thus, we are talking about the directed synthesis of organic compounds with predetermined properties and, as a rule, having physiological activity for the purpose of using the latter for various purposes, including as medicaments. Considering the fact that the synthetic potential of the catalytic olefination reaction is extremely wide and the scope of its application covers both aliphatic and aromatic aldehydes and ketones, and also the ease with which conversions are carried out, high yields of the target products allow the catalytic olefination reaction to be used as a convenient tool in organic synthesis [1-7].

The catalytic olefination reaction is based on the conversion of the C=O group of the carbonyl compound to a C=C group. The use of various polyhaloalkanes along with geminal dihalogen-substituted alkenes made it possible to obtain also functionally substituted haloalkenes. During the reaction, only symmetrical azines are formed as a by-product and nitrogen evolution is observed. It should be noted that the catalytic olefination reaction has a number of advantages over the classical olefination methods. The use of various polyhaloalkanes allows to synthesize a large number of halogen- and functionally substituted alkenes (Scheme 1)[8-13].

2. EXPERIMENTAL

Scheme 1.General scheme of catalytic olefination reaction.

In contrast to the foregoing, we found that, during the reaction of N-substituted hydrazones, instead of the expected dichloroalkene, the derivatives of dichlorodiazobutadiene were formed (Scheme 2).
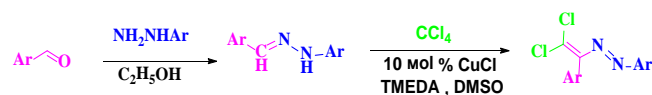
Scheme 2.Scheme of catalytic olefination reaction of N-substituted hydrazones.

The new compounds obtained in the catalytic olefination reactions (scheme 2) have some advantages over the products of the previous reactions. Thus, the presence in them of two functional groups, both the geminal dihalogen double bond and the azo- group conjugated with it (dichloroazobutadiene) allows us to

speak of their great importance from the point of view of organic synthesis. It should be notedthat there is a little information in the literature on the synthesis and reactivity of diazadienes, although they are already widely used as indispensable syntons in various heterocyclization reactions [14]. It should be noted that these compounds show high physiological activity and also have broad prospects for use as azo derivatives in analytical chemistry .

Taking into account all the above, we investigated the antimicrobial properties of the simplest of the compounds synthesized according to scheme 3 - (E) -1- (2,2-dichloro-1-phenylvinyl) -2-phenyldiazenine.
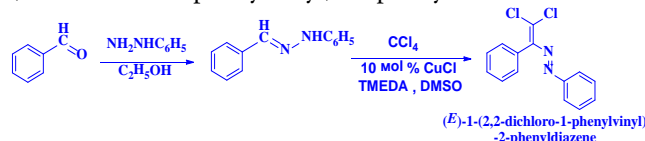
Scheme 3. Synthesis scheme of (E) -1- (2,2-dichloro-1-phenylvinyl) -2-phenyldiazenine.

The structure of the obtained compound was confirmed on the basis of ^{1}H and ^{13}C NMR spectra. Along with this, its single crystal was obtained and the structure of the compound was confirmed again by the X-ray diffraction method.
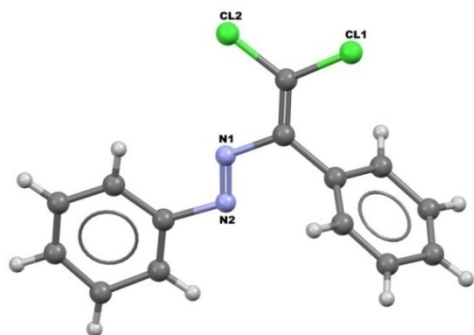
Fig. 1. Molecular structure of (E) -1- (2,2-dichloro-1-phenylvinyl) -2-phenyldiazenine

In previous studies the role of halogen bonds in the synthesis and design of 1,4-bis (dichlorovinyl) tetrafluorobenzenes, obtained on the basis of the catalytic olefination reaction was studied by the X-ray diffraction method [10].The presence of intermolecular noncovalent CI ···CI bonds in the newly synthesized (E) -1-(2,2-dichloro-1-phenylvinyl)-2-phenyldiazene was also proved by the X-ray diffraction method (Fig. 2).

Taking into account all the above, we investigated the antimicrobial properties of the simplest synthesized compound - (E) -1- (2,2-dichloro-1-phenylvinyl) -2-phenyldiazenine. To this end, 1% solution of (E) -1-

(2,2-dichloro-1-phenylvinyl) -2-phenyl-diazenine in ethyl alcohol is diluted in distilled water in the ratios of 1: 100, 1: 200, 1: 400, 1: 600 , 1: 800 (1,2,3,4).
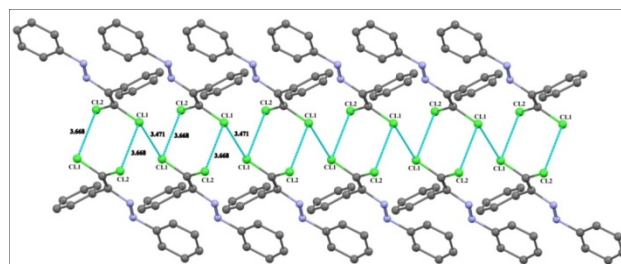
Fig. 2. Non-covalent CI-CI bondsare indicated by dashed lines

The antimicrobial properties of (E) -1- (2,2-dichloro-1-phenylvinyl) -2-phenyldiazenine have been studied in comparison with widely used drugs such as ethyl alcohol, furacilin and nitrofungin. Gram-positive microorganism - Staphylococcus aureus, gram-negative - Pseudomonas aeruginosa, Escherichia coli, fungal - Candida albicans were used as a test culture. For the inoculation of bacteria, MPA (meat-peptone agar), and for the inoculation of fungi - Saburo agarwere used [15-19]. Bacteria inoculationwas carried out under the conditions of a thermostat, for 24 hours at a temperature of plus 37 ° C, and for fungi for 48 hours at a temperature of 28 ° C. For each test glass, one drop of emulsion was added, containing 500ml of microbial particles per 1ml, and inoculation was carried out every 10-20 minutes for 1 hour. The antimicrobial properties of the synthesized compound are shown in Table 1, and the control compounds in Table 2.

According to the analysis of the data of Table 1, the synthesized compound has a strong antimicrobial effect on the investigated microorganisms, and for all investigated microorganisms in the samples 1,2,3 regardless of time. So, even at a dilution of 1: 800 (sample 4), it completely destroys staphylococcus and E. coli after 20 minutes. With respect to candida, a decrease in the development rate after 10 minutes at a ratio of 1: 200 and 20 minutes at 1: 400 was observed.

The action of ethanol used as a solvent is shown in Table 2.

The antimicrobial properties of this compound were also studied by the method of disk diffusion. A suspension was prepared from the daily culture (containing 1ml of 1 ml\g of microbial cells). Further, in a Petri dish with MPA, this suspension was added and distributed within this nutrient medium.

Table 1. Antimicrobial properties of (E) -1- (2,2-dichloro-1-phenylvinyl) -2-phenyl-diazenine

Test cultures	Exposure time (min)	Synthesized compound			
		1	2	3	4
St. aureus	10	-	-	-	+
	20	-	-	-	-
	40	-	-	-	-
	60	-	-	-	-
Ps. aeruginoza	10	-	-	-	+
	20	-	-	-	+
	40	-	-	-	-
	60	-	-	-	-
E. coli	10	-	-	-	+
	20	-	-	-	-
	40	-	-	-	-
	60	-	-	-	-
Cand. albi- cans	10	-	-	+	+
	20	-	-	-	+
	40	-	-	-	+
	60	-	-	-	+

Note: 1 (1: 100), 2 (1: 200), 3 (1: 400), 4 (1: 800) dilution ratios "+" Availability of inoculation "-" lack of inoculation

Table 2. Antimicrobial properties of control compounds

Testcultures	Exposure time (min)	Control compounds											
		ethanol				furacilin				nitrofungin			
		1	2	3	4	1	2	3	4	1	2	3	4
t. aureus	10	-	+	+	+	-	+	+	+				
	20	-	+	+	+	-	+	+	+				
	40	-	+	+	+	-	+	+	+				
	60	-	+	+	+	-	+	+	+				
Ps. aeruginoza	10	+	+	+	+	+	+	+	+				
	20	-	+	+	+	+	+	+	+				
	40	-	+	+	+	+	+	+	+				
	60	-	+	+	+	+	+	+	+				
E. coli	10	+	+	+	+	-	+	+	+				
	20	-	+	+	+	-	+	+	+				
	40	-	+	+	+	-	+	+	+				
	60	-	+	+	+	-	+	+	+				
Cand. albi cans	10	+	+	+	+	+	+	+	+	+	+	+	+
	20	+	+	+	+	+	+	+	+	+	+	+	+
	40	-	+	+	+	+	+	+	+	-	+	+	+
	60	-	+	+	+	+	+	+	+	-	+	+	+

Excess liquid was removed by pipetting and the cup was further dried in a thermostat for 10-15 minutes. Sterile discs of filter paper impregnated with our preparation are placed in the border zone and placed in a thermostat for cultivation for 18-24 hours at a temperature of 37 ^{0}C. So this preparation in

Staphylococcusaureus, Pseudomonasaeruginosa, Escherichia coli formed a 30 mm sterile zone, in Candidaalbicans - 20 mm sterile area. Thus, the (E) -1- (2,2-dichloro-1-phenylvinyl)-2-phenyldiazenine synthesized by us is an active bactericidal and fungicidal preparation.

3. RESULTS AND DISCUSSION

Synthesis of phenylhydrazones (general procedure)

Ethanol (20-50 ml) and acetic acid (1 ml) are added to a three-necked, round bottom flask containing phenylhydrazine (2 moles). A back condenser, a dropping funnel and a thermometer are attached to the flask. Using a dropping funnel, 2.1 mole of aldehyde is added and the reaction mixture is heated by stirring. The temperature is brought to 78 ° C and the mixture is boiled for 5-10 minutes. Then the reaction mixture is cooled to the room temperature and 50 ml of water is added. Mixture is filtered. If necessary, the product residuesare washed with water. The resulting hydrazone is dried at room temperature (15-20 hours). Data of 1H NMR and13C spectra correspond to the literature data.

4. CONCLUSION

Catalytic Olefination Reaction (General Procedure)

20 ml of DMSO, (581 mg: 2.5 mol / eq) of TMEDA are added to a flask containing 2 moles of phenylhydrazone. Next, CuCl (6 mg, 3 mole%) is added. Finally, CCl4 (7-10 mol / eq, 2.2-3 g) is added. The magnetic stirrers are lowered and the reaction of TLC is checked. As a rule the reaction is completed after 1.5-3 hours. The reaction mixture is moved into the separatory funnel(3 * 15m). After washing with water the organic phase (3 * 50 ml) is washed again with a saturated solution of NaCl (1 * 50 ml). Dried with Na_2SO_4 ($MgSO_4$), filtered and dichloromethane is distilled in vacuum. The resulting product is dissolvedin ethyl alcohol, cooled in a flask and crystals are obtained, respectively. The yield is 65-75%.

Used equipment:

1H and 13C NMR spectra were recorded in Bruker Advance 400 (operating speed, respectively, of 400.1 Mhs and 100.6 Mhs) spectrometer in $CDCl_3$ and DMSO-d6. $SiMe_4$is used as the internal standard. TLC was conducted on a UB-25 silicogenic plate, and the acidified $KMnO_4$ and UV lamp were used for spot sharpness. The column chromatography was carried out with Merk silicagel (63-200).

5. REFERENCES

1. Shastin A.V., Korotchenko V.N., Nenajdenko V.G.,Balenkova E.S /The news of AN, Chemical series,1999,№11,p.2210-2211

2. Shastin A.V., Korotchenko V.N., Nenajdenko V.G., Balenkova E.S.. /Tetrahedron, 2000, V.56, P.6557-6563

3. Nenajdenko V.G., Shastin A.V, Korotchenko V.N, Balenkova E.S. /The news of AN, Chemical series,2001,№6,p.1003-1006.

4. Nenajdenko V.G., Shastin A.V., Muzalevsky V.M., Balenkova E.S //The news of AN, Chemical series,2004,№11, p.2538-2540.

5. ShastinA.V.,KorotchenkoV.N.,NenajdenkoV.G.,BalenkovaE.S/Synthesis, 2001, p.2081-2084

6. NenajdenkoV.G.,LenkovaO.N.,ShastinA.V.,Balenkova E.S. /Synthesis,2004,P.573-577.

7. Nenajdenko V.G, Shastin A.V, Golubinsky I.V, Lenkova O.N, Balenkova E.S. /The news of AN, Chemical series, 2004, №1, p. 218-222.

8. V.M Muzalevsky, E.S Balenkova, A.V Shastin, N.G Shikhaliev, A.M Maharramov, N.V Gurbanova, V.G Nenajdenko / Bulletin ofMoscow University, Chemistry, 2011, v. 52, № 6, p. 456-460.

9. V.M Muzalevsky, N.G Shikhaliev, A.M Maharramov, N.V Gurbanova, S.J Geydarova, E.S Balenkova, A.V Shastin, V.G Nenajdenko / The newsof RAN,2013, № 3, p. 677–681

10.V.M.Muzalevskiy, A.V.Shastin, A.D.Demidovich, N.G.Shikhaliyev, A.M.Magerramov, V.N.Khrustalev, R.D. Rakhimov, S.Z. Vatsadze ,V.G. Nenajdenko /Beilstein Journal of Organic Chemistry,p. 2072-2078, 2015

11.V.M. Muzalevskiy, A.V. Shastin, N.G.Shikhaliyev, A.Maharramov, A.N.Teymurova, V.Q.Nenaydenko / Tetrahedron. Volume 72, Issue 45, Pages 7159–7163, 10 November 2016

12.V.G. Nenajdenko, A.V. Shastin, V. M. Gorbachev, S.V. Shorunov, V..M. Muzalevskiy, A.I. Lukianova, P.V.Dorovatovskii, V.N. Khrustalev / ACS Catal., 7 (1), pp 205–209, 2017

13.V.M. Muzalevsky, N.G Shikhaliev, A.M Maharramov, E.S Balenkova, A.V Shastin, P.V Dorovatovsky, Y.Z. Zubavichu, V.N Khrustalev, V.G Nenajdenko / The news of AN, Chemical series, vol.65, № 6, p. 1541-1544, 2016

14.V.G. Nenajdenko, A.V. Shastin, V. M. Gorbachev, S.V. Shorunov, V..M. Muzalevskiy, A.I. Lukianova, P.V.Dorovatovskii, V.N. Khrustalev / ACS Catal., 7 (1), pp 205–209, 2017

15.C.A.Lipinski, / Drug Discovery Today: Technologies, vol.1, №4, pp. 337-341, 2004. doi.org/10.1016/j.ddtec.2004.11.007

16.M.J.Macielag, / T.J.Dougherty and M.J.Pucci, Eds., pp. 801-802, 2012. doi.org/ 10.1007/978-1-4614-1400-1_24

17.A.Israyilova, S.Buroni, F.Forneris, VC Scoffone, NQ Shixaliyev, G.Riccardi et al PLoS ONE 11 (11), 2016, doi:10.1371/journal.

18.A.U.Rahman, M.I.Choudhary, W.J.Thomsen, Bioassay Techniques for Drug Development, vol. № 22, HarwoodAcademicPublishers, Netherland, 2001.

19.Tirkey, S.Mishra, H.R.Dash, S.Das and etc. / Journal of Org.Chemistry v.732, p.122-129, 2013, doi.org/10.1016/j.jorganchem.2013.02.020.

THE QUANTUM CHEMICAL CALCULATIONS ON MODELLING OF Fe_3O_4 NANOCLUSTERS, FUNCTIONALIZED WITH DIAZACROWN ETHER

M.A. Ramazanov[1], A.M. Maharramov[1], Z.O. Gakhramanova[2], N.S.Nabiyev[1],

U.A. Hasanova[1], G.C.Abbasova[1], S.F. Hajiyeva[1], F.V.Hajiyeva

[1]Baku State University, Z.Khalilov 23 Str., Baku, Azerbaijan
[2]RI Geotechnological properties of gas oil and chemistry, Azadliqave. 20, Baku, Azerbaijan
E-mail: mamed_r50@mail.ru

In the paper we report of the successful synthesis of hydroxysubstituteddiazacrown ether that forms the supramolecular ensemble with magnetite nanoparticles. Via series of molecular-mechanical, molecular dynamics and quantum chemical calculations, it was implemented the modelling of Fe_3O_4nanocluster with diazacrown ether. Based on the results of the analysis of quantum chemical calculations, which were performed using the semiempirical PM3 and ZINDO/1, were found the energy parameters, characterizing the electron spatial structure of the non-valence diazacrownether@Fe_3O_4 complexes. Thequantum chemical calculations of the modelling of Fe_3O_4nanoclusters with diazacrown ether are in good correlation with experimental data, proving the obtaining of supramolecular ensemble of diazacrown ether with magnetite nanoparticles.

Keywords:diazacrown ethers, supramolecular ensemble, magnetite nanoparticle, quantum chemical calculations

1.INTRODUCTION

Crown ethers have unique properties, characteristic to supramolecular compounds that are capable to form host-guest complexes [1]. Azacrown ethers are currently successfully used in various fields of science and technology, as a phase transfer catalysts in organic synthesis [2], as a highly selective ligands for the selective binding of metal cations in analytical chemistry [3], for creating contrast agents for the diagnosis in magnetic resonance imaging and therapeutic purposes in medicine [4]. Functional derivatives of azacrown compounds, binding with lanthanides (III) ions, are widely used in radiodiagnostics [5, 6]. Furthermore, azacrown compounds are used as reagents in biochemical studies [7].

It is known that crown ethers can exhibit properties of the natural membrane-active antibiotics, due to ionophoric [8] features of macrocyclic cavity, able to bind cations by ion-dipole, dipole-dipole non-covalent bonds that leads to changes in membrane permeability, membrane potential, and, consequently, to cell disruption [9]. The concept of supramolecular compounds and nanostructures has a lot in common. The basic principle of the formation of supramolecular assemblies and nanoparticles is the principle of self-assembly and intermolecular recognition. [10]

The use of magnetite-containing nanocapsules, by applying an external magnetic field, is the promising approach for the targeting drug delivery. However, the application of magnetite nanocapsules in living organisms requires strict control of nanocapsules' surface to prevent nonspecific adsorption of plasma proteins, which leads to the rapid elimination from the blood stream, by modification with various compounds,preserving nanocapsulesfrom the aggregation [11,12,13,14].

The design of the macrocycle molecule, capable to forming supramolecular assemblies with metal nanoparticles, serving as stabilizers, and thus increasing biological activity of macrocycles, is a matter of scientific and practical interest. During designing nanostructures with desired functional properties, it is important to consider the coordinates of each atom. This problem is successfully can be solved by mathematical modelling [15, 16, 17]. In the bulk metallic materials the position of atoms in the crystal lattice sites is strictly determined, i.e., there is a regularity and order of a simple translation of the unit cell, whereas in the complex nanostructure the organization of atoms must be specified. Therefore, it is important to clarify, how the organization of atoms will affect the properties and stability of nanostructure.

There are several methods for calculating the energy of atomic bonds in the structure; the most reliable is *ab*

initio density functional method. However, existing software products (GAMESS, Abinit, FHI and etc.) are quite effective in the mathematical modelling of the assembly of nanostructures, consisting of few atoms [18]. In addition, it is not clear, whether it is possible to predict the functional properties of nanostructures, on the basis of the calculation of the total energy and the binding energy of atoms. In this context, the consideration of new approaches to the prediction of stability and functional properties of nanostructures is quite important problem from theoretical and practical points of view.

Construction of nanostructures involves a technology of manipulation on the atomic level. In order to calculate the stability of designed nanostructures with specified functional properties, there is a need to use the approaches of quantum mechanics. In the paper we report of synthesis of hydroxysubstituteddiazacrown ether that forms the supramolecular ensemble with magnetite nanoparticles, and via series of molecular-mechanical, molecular dynamics and quantum chemical calculations, present the modelling of Fe_3O_4 nanoclusters with diazacrown ether.

All chemicals, used in the synthesis, were of analytical grade and used as received. Ethylenediamine, 1,3-dichloro-2-propanol, salicylaldehyde were purified by distillation under reduced pressure, created by water pump. $FeCl_3 \cdot 6H_2O$, $FeSO_4 \cdot 7H_2O$, NH_4OH (25 %), were purchased from Sigma-Aldrich (Taufkirchen, Germany)

The synthesis of 1,13-Diaza-5,9-dioxa-7-hydroxy-3,4:10,1-dibenzocyclopentadecan was performed as described by U. Hasanova et al.[19]

Synthesis of nanocluster by functionalization of Fe_3O_4 with diazacrown ether (diazacrownether@Fe_3O_4 NPs) was carried out as shown by U. Hasanova et al. [19]

The functional groups, present in the powder samples of diazacrownether@Fe_3O_4 NPs, were identified by Fourier Transform Infrared (FTIR) spectroscopy. FTIR spectra were recorded on a Varian 3600 FTIR spectrophotometer in KBr tablets. The spectrum was taken in the range of 4000-400 cm^{-1} at room temperature.

SEM analysis of prepared samples of diazacrownether@Fe_3O_4 nanoparticles were taken on Field Emission Scanning Electron Microscope JEOL JSM-7600F at an accelerating voltage of 15.0 kV, SEI regime.

2. RESULTS AND DISCUSSIONS

Were carried out the series of molecular-mechanical, molecular dynamics and quantum chemical calculations on modelling Fe_3O_4 nanoclusters with diazacrown ether, simulating the behaviour and properties of biological molecules – siderophores, secreted by bacteria [20,21]. By means of molecular mechanical calculations were found the low-energy conformations of these compounds [22]. Molecular mechanical model of diazacrown ether was compiled on the basis of its chemical structure. Initial structural options were based on the ideal values of bond angles and lengths of chemical bonds. After minimizing the total energy in the variation of geometrical parameters, it was revealed that the conformational possibilities of diazacrown ether are severely limited. Preference for low-energy single spatial structure is mainly determined by the absence of steric strain. The contribution of non-covalent stabilizing bonds is not too pronounced. Optimal 3D spatial structure of diazacrown ether molecule is presented in the Fig. 1(a).
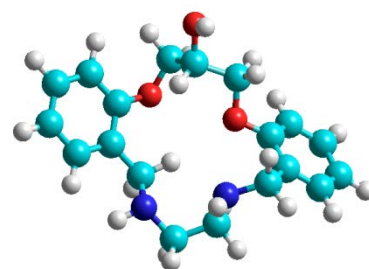
a)
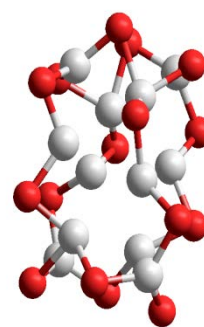
b)

Figure 1. 3D spatial structure: a) diazacrown ether molecule; b) Fe_3O_4 nanocluster

In drawing up the calculation model of Fe_3O_4 nanoclusters were taken into account the different valence states of iron atoms. In drawing up the initial options for optimizing the three-dimensional structure of Fe_3O_4 nanoclusters, were also used the ideal values of bond angles and chemical bonds' lengths, corresponding to different valence states of iron atoms. Calculations showed that nanocluster Fe_3O_4 also has a fairly rigid three-dimensional structure. Low-energy 3D structure of Fe_3O_4 nanocluster is shown in Fig. 1(b).

The FTIR spectra of pure diazacrown ether (1), diazacrownether@Fe_3O_4 (2) and pure Fe_3O_4 nanoparticles (3) are given in Fig.2. As it seen from FTIR spectra (1), the wide band at 3330-3350 cm^{-1}, corresponding to $\nu(OH)$ and $\nu(NH)$ of diazacrown ether, is not revealed on the spectrum (2) of diazacrownether@Fe_3O_4. This fact evidenced that the main chelation sites of diazacrown ether with Fe_3O_4 nanoparticles occur via hydroxyl and NH groups of the diazacrown ether ring. The weakening of intensity of strong band at 1455 cm^{-1}, corresponding to the NH groups, also proves that the coordination occurs through NH group. At the same time the intense band at 1250 cm^{-1} and 1034 cm^{-1} ($Ar-O-CH_2$) of diazacrown ether (1) are shifted to 1240 cm^{-1} and 1010 cm^{-1} region on the spectrum (2). These indicate the involving of macrocycle's oxygen atoms in coordination process at less extend. Thus, the IR spectral results provide strong evidences for the multiple chelation sites of diazacrown ether with surface of magnetite NPs.
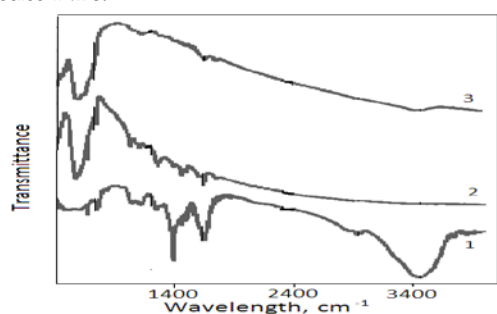
Figure 2. FTIR spectra:1) pure diazacrown ether, 2) diazacrownether@Fe_3O_4, 3) pure Fe_3O_4

SEM image of diazacrownether Fe_3O_4, presented in fig. 3, demonstrates that the obtained nanoparticles are homogenous, with average size in the range from 5.5-13 nm. The agglomerations of nanoparticles are observed.
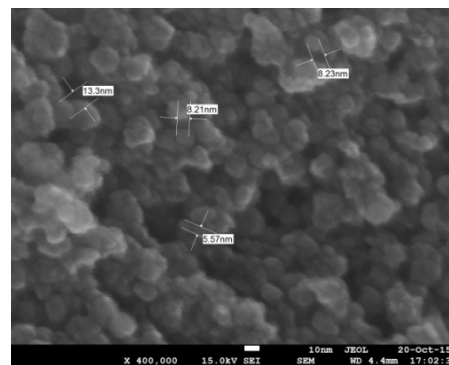
Figure 3. SEM image of diazacrownether@ Fe_3O_4

Using the coordinates of the atoms in the low-energy structures, were conducted the quantum-chemical calculations of the electronic structure of diazacrownether@Fe_3O_4. When optimizing the electronic structure, some geometrical parameters were also optimized. As a result of quantum chemical calculations, have been found the energy parameters, characterizing the electronic and spatial structures of diazacrownether@Fe_3O_4. By analysing these parameters, can be represented the stabilization options of complexes of diazacrownether@Fe_3O_4 by means of valence and non-valence bonds. Atomic groups with significant partial charges, interacting with each other, can play a determining role in the convergence of the components, subsequently ensuring the stability of the complexes. Spatial features of the components are also very important. Only spatially complementary components can form stable complexes. It can be expected that the possible stable complexes with minimum number of components, on the basis of the received data, can consist of one molecule of diazacrown + one Fe_3O_4 nanocluster. Spatial feature of this complex is most favourable for the implementation of stabilizing electrostatic and non-covalent interactions.
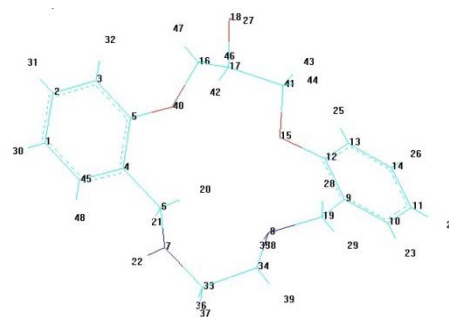
Figure 4. Numbering of atoms in calculation scheme of diazacrown molecule

Table 1. Effective charges (e) of atoms of the diazacrown ether molecule (in the unit of elementalcharge)

N	Atom	Effective charges (e)	N	Atom	Effective charges (e)
1	C	-0.070339	25	H	0.064169
2	C	-0.058576	26	H	0.062687
3	C	-0.086365	27	H	0.193923
4	C	-0.002838	28	H	0.060545
5	C	0.116762	29	H	0.041439
6	C	-0.018886	30	H	0.057236
7	N	-0.336402	31	H	0.060467
8	N	-0.334100	32	H	0.061681
9	C	-0.009606	20	H	0.093298
10	C	0.058818	21	H	0.041900
11	C	0.069235	35	H	0.161015
12	C	0.121828	36	H	0.041042
13	C	0.081586	37	H	0.051986
14	C	0.057433	38	H	0.061788
15	O	0.248834	39	H	0.036615
16	C	0.023438	22	H	0.153389
17	C	0.077988	23	H	0.058690
18	O	0.319287	42	H	0.065719
19	C	0.008736	43	H	0.058654
33	C	0.006014	44	H	0.048322
34	C	0.006750	24	H	0.059913
40	O	0.253332	46	H	0.068883
41	C	0.017318	47	H	0.068933
45	C	0.057484	48	H	0.054993

Based on these results, it can be assumed that the possible stable complexes, with a minimum number of components bind to each other via non-covalent bonds, can be realized in the following ratio - N diazacrown:Fe_3O_4, (where N = 1-4). The spatial structure of such complexes can be stabilized in the realizing of non-valence electrostatic interactions between atoms and groups of diazacrown molecules and Fe_3O_4 nanocluster. Partial charges of diazacrownether's atoms and Fe_3O_4 nanoclusters are shown in Tables 1 and 2, respectively. As can be seen from Table 1, the most significant negative charges are on the atoms N_8, N_9, O_{15}, O_{18} and O_{40}. The positive partial charges are distributed relatively evenly with moderate values. The highest high positive charges appear at atoms H_{22}, H_{27}, and H_{35}.
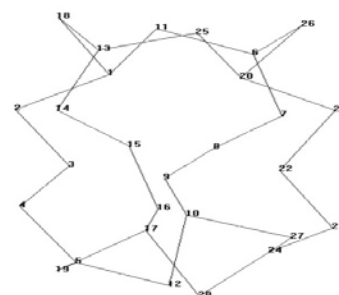
Figure 5. Numbering of atoms in calculation scheme of Fe_3O_4 nanocluster

As seen from Table 2, iron atoms are depleted in electron density, and extent of depletion depends on iron atoms' valence states, and all oxygen atoms are negatively charged. The relative position of the atoms in the various components that may lead to significant electrostatic interaction does not impede the implementation of effective non-bonded contacts between atoms of diazacrown ether and Fe_3O_4 nanocluster.

Table 2. Effective charges (e) of atoms of the Fe_3O_4 nanocluster (in the unit of elementalcharge)

N	Atom	Effective charges (e)	N	Atom	Effective charges (e)
1	Fe	0.264408	2	O	-0.285770
6	Fe	0.474189	9	O	-0.144283
13	Fe	0.443934	16	O	-0.263625
20	Fe	0.246953	18	O	-0.048819
3	Fe	0.229802	19	O	-0.135449
5	Fe	0.310576	4	O	-0.291968
8	Fe	0.097059	11	O	-0.301045
10	Fe	0.291445	12	O	-0.212996
15	Fe	0.328068	21	O	-0.286839
17	Fe	0.145245	23	O	-0.312292
22	Fe	0.254473	25	O	-0.298205
24	Fe	0.359447	26	O	-0.031798
7	O	-0.282503	27	O	-0.167260
14	O	-0.305837	28	O	-0.076909

Therefore, the most stable spatial structure of the complex can be achieved, when there are maximum number of non-covalent stabilizing contacts between atoms of diazacrown ether and nanocluster Fe_3O_4, at appropriate favourable relative position of positively and negatively charged atomic groups. This fact greatly reduces the possibility of implementing of the complex structural variants. Initial calculation options ratios: diazacrown/Fe_3O_4 nanocluster - 1:1, 2:1, 3:1, 4:1 are designed so that the maximum numbers of atoms of the components were in the range of Van der Vaals radii. Thus, the mechanical model of the constituting

11

components was applied. By optimizing these options were received the most probable spatial structures of complexes. The atomic coordinates of these structures are used in the preparation of the initial options for quantum chemical calculations.

Quantum chemical calculations were performed, using the semiempirical PM3 and ZINDO/1.[23-25]. The energy parameters and the parameters, characterizing the electron spatial structure of the non-valence diazacrownether @Fe_3O_4 complexes were found.

Table 3. Energy parameters of diazacrown ether, Fe_3O_4 nanocluster and diazacrownether@Fe_3O_4 (kcal/mole)

N	E_t (total energy)	E_b(bonding energy)	E_e(electron energy)	E_{cc}(repulsion energy)
Fe_3O_4	-253754.515 -334978.001	-2991.784 -1534.423	-1558983.882 -1684268.790	1305229.367 1349290.789
Diazacrown	-89221.716 -134224.862	-4816.127 -14245.420	-758227.735 -863788.943	669006.019 729564.081
Diazacrownether@Fe_3O_4 (1:1)	-343010.951 -469313.618	-7842.631 -15890.600	-3405998.855 -3651177.869	3062987.904 3181864.251
Diazacrownether@Fe_3O_4 (2:1)	-430292.260 -601483.628	-13011.766 -30852.754	-5513598.641 -5873425.767	5083306.382 5271942.140
Diazacrownether@Fe_3O_4 (3:1)	-518594.802 -734722.132	-18055.428 -45497.611	-8475797.358 -8966340.803	7957202.556 8231618.671
Diazacrownether@Fe_3O_4 (4:1)	-606859.250 -867941.431	-23060.995 -60123.262	-11463196.145 -12073071.635	10856336.895 11205130.204

Table 3 shows the energy parameters of free components (1st and 2nd row) and related complexes (calc. top by PM3, lower by ZINDO/1). The analysis of these parameters allows coming to the conclusion that non-valence complexes of diazacrownether@Fe_3O_4 are energetically favourable and having sufficient stabilization energy.

The most significant reduction in total energy and the binding energy of the complex formation occurs at the 1:1 ratio, $\Delta E_{t1} + 1 = 34.676$ kcal/mole (according to PM3), 110.755 kcal/mole (according to ZINDO/1). In the formation of the complex there is a slight change in the component structures; the redistribution of

electron density, associated with the approach of diazacrown atoms to the Fe_3O_4 atoms, does not create the conditions that are necessary for breaking chemical bonds and restructuring. In other complexes with the increasing of the number of diazacrown molecules occurs the increase of the binding energy of complexes, but the reduction of the total energy is not particularly noticeable. In accordance to 3D structure of optimised nanostructure the sizes of diazacrownether@Fe_3O_4 nanostructures in the ratios of 1:1; 2:1; 3:1; 4:1 are 1.3 nm; 1.8 nm; 2 nm; 2.3 nm correspondingly and very well correlates with the results, obtained from XRD analysis.

a)   b)
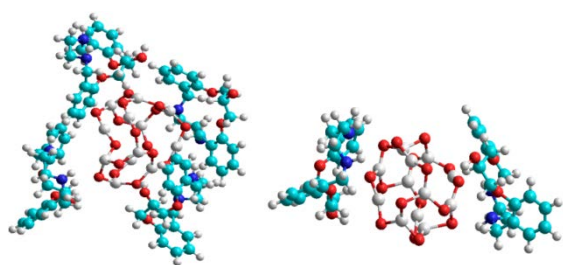
Figure 6. 3D spatial structure: a)diazacrownether@Fe_3O_4 (2:1); b) diazacrownether@Fe_3O_4 (4:1)

3. CONCLUSION

The successful synthesis of hydroxyl substituted diazacrown ether that forms the supramolecular ensemble with magnetite nanoparticles was carried out. Based on the results of the implemented analysis of series of molecular-mechanical, molecular dynamics and quantum chemical calculations, it can be assumed that non-covalent complexes of diazacrownether@Fe_3O_4 in different formulations can be stabilized by non-covalent and electrostatic interactions. The complex of diazacrownether@Fe_3O_4 at 1:1 ratio is energetically more stable. This suggests that the adsorption process of diazacrown ether molecules on the surface of Fe_3O_4 nanocluster can compete with the process of adhesion of Fe_3O_4 nanoparticles. The formation of more complex systems, which include more than 4 molecules of diazacrown, is not competitive with respect to the adhesion of Fe_3O_4 nanoparticles in terms of energy.

4. REFERENCE

1. Steed J.W., Atwood J.L.,Supramolecular chemistry,2nd edition/John Wiley & Sons, Ltd., Chapter 1.7, p.27-38, 2009.
2. Schettini R., Riccardis F.De, Della Sala G., Izzo I. /J. Org. Chem., 2016, 81(6), p. 2494–2505.
3. Lehn J.M. Supramolecular Chemistry Concepts and Perspectives, Wiley-VCH, Weinheim, Chapter 2, pp.11-24, 1995
4. Oukhatar F., Même S., et al./ ACS Chem. Neurosci., 2015, 6(2), p. 219–225.
5. Oueslati I., Sa´Ferreira R.A., et al./ Inorganic Chemistry, 2006, 45(6), p. 2652-2660.
6. Chhikara B.S., Kumar S.,et al./ Chemical Biology Letters, 2014, 1(2), p. 77-103.
7. Späth A., König B/Beilstein J. Org. Chem.,2010, 6(32), p. 1-111.
8. Tempelaars M.H., Rodrigues S., Abee T/ Applied and environmental microbiology, 2011, 77(8), p. 2755–2762.
9. Enache I.V., Mutihac L., et al./J Incl Phenom Macrocycl Chem, 2011, 71(3), p. 537–543.
10. Piccinini E., Pallarola D., Battaglinic F., Azzaroni O./Mol. Syst. Des. Eng., 2016, 1, p. 155-162.
11. Tartaj P., Morales M. P., et al./ Handbook of Magnetic Materials, Elsevier, Amsterdam, p. 403-482,(2006)
12. Latorre M., Rinaldi C. / P R Health Sci J., 2009, 28(3), p. 227-238.
13. Saboktakin M.R., Tabatabaie R.M. et al./ Carbohydrate Polymers, 2010, 80(3), p. 695-698.
14. Saboktakin M.R., Tabatabaie R.M., et al./ Carbohydrate Polymers, 2010, 81(2), p. 372-376.
15. Melnik R.V.N., Kotsireas I. S./Advances in Applied Mathematics, Modeling, and Computational Science, Fields Institute Communications, 2013, 66, Springer, New York, p. 1–10.
16. Melnik R.V.N., / Nanoscale Systems: Mathematical Modeling, Theory and Applications, 2013, 2, p. 1–9.
17. Maharramov A.M., Alieva I.N., Abbasova G.D., Ramazanov M.A., Nabiyev N.S., Saboktakin M.R./ Journal of Nanomaterials and Biostructures, 2011, 6(2), p.463-472.
18. Band Y.B., Avishai Y., Quantum Mechanics with Applications to Nanotechnology and Information Science, 1st Edition, Chapter 15, Academic Press, Elsevier,2012, p. 871-888.
19. Hasanova U.A., Ramazanov M.A. et al./J Incl Phenom Macrocycl Chem, 2016, 86(1), p.19-21.
20. Raymond K.N./ Pure and Applied Chemistry, 1994, 66(4), p. 773-781.
21. Hasanova U., Ramazanov M., et al./ Chemical Engineering Transactions, 2016, 47, p. 109-114.
22. Kamachi T., Yoshizawa K./ J Chem Inf Model, 2016, 56(2), p. 347-353.
23. Stewart J. J. P. / J. Comput. Chem., 1989, 10(2), p. 209–220.
24. Ridley J., Zerner M./Theoret. Chim. Acta,1973, 32(2), p. 111 – 134.
25. Sivakumar P. M., Kodolov V.I., Zaikov G. E., Haghi A. K., Nanostructure, Nanosystems, and Nanostructured Materials: Theory, Production and Development, Apple Academic Press, Chapter 6, 2013, p. 231-287.

13

STRUCTURE AND THERMIC PROPERTIES OF POLYMER NANOCOMPOSITES ON THE BASIS OF POLYPROPYLENE AND SILVER SULPHIDE NANOPARTICLES PP/Ag2S

A.M.MAHARRAMOV, M.A.RAMAZANOV, S.G.NURIYEVA, F.V.HAJIYEVA

Baku State University, Radiation and influence in surrounding the environment Scientific research laboratory, Baku, Azerbaijan

The morphology of nanocomposites based on polypropylene and silver sulfide synthesized by ultrasound and microemulsion techniques and distribution of silver sulfide nanoparticles in polymer matrix was investigated by AFM and SEM methods. Absorption spectra was analysed by UV spectroscopy and also observed redshift phenomenon. During thermal analysis it was found out that formation of Ag_2S nanoparticles in polypropylene matrix effect to destruction proses occurring in nanocomposites. Data obtained from thermogravimetric analysis show that with adding nanoparticles initial decomposition temperature shifted to lower temperatures.

Keywords: nanocomposite, termic properties, silver sulphide nanoparticles.

1. INTRODUCTION

Over the last few years, nanocomposite materials based on thermoplastic polymer and various types of inorganic fillers have been an area of intensive research for transducer technique [1-3]. It should be noted that, nanocomposites obtained on the basis of inorganic filler and organic polymer combine numerous advantages of organic and inorganic components and leads to substantial improvement of the material's properties [4-6].

For the practical application of nanocomposite materials with a low concentration of filler in a polymer matrix, high thermal stability plays an important role.

The present article considers the depending of structure, morphology and thermal properties of

PP/Ag_2S polymer nanocomposites on concentration of Ag_2S. The PP/Ag_2S nanocomposites based on nonpolar PP and semiconductive silver sulfide with unique optic properties was synthesized with new method which combined ultrasound and microemulsion techniques [7]. The properties of Ag_2S-based polymer nanocomposites are very sensitive to synthesis route and mostly depend on structure of polymer. Thus, silver sulfide Ag_2S play the role of structure-forming centers for the polymeric macromolecules, furthermore, the polymer matrix in turn stabilizes Ag_2S nanoparticles.

2. EXPERIMENTAL

For research used the powder of isotactic polypropylene powder (M 250000g/mol), silver nitrate

($AgNO_3$), sodium sulfide (Na_2S), toluene ($C_6H_5CH_3$), $C_{12}H_{25}SO_4Na$ - lauryl (dodecyl) sodium sulphate, H_2O - distilled water.

For the synthesis of nanocomposite PP/Ag2S was used a combinational method which combines the application of ultrasound and microemulsion methods. Were prepared aqueous solutions of 0.005 M, 0.0025 M, of the $AgNO_3$ and Na_2S salts. 0.25 g of polypropylene powder was dissolved in 50 ml of toluene. 5 ml of the respective aqueous salt solution in the presence of 0.01 g of sodium lauryl sulfate was mixed with 25 ml of toluene/PP solution. Every separately taken microemulsion $AgNO_3$/toluene+PP and Na_2S/toluene+PP were treated by ultrasound for 20 minutes (0.6 cm diameter; Ti-tip; 20kHz; 60W/cm2) at a temperature of 30^0C, by use of a cooling bath. Then, a microemulsion containing Na_2S/PP+toluene was slowly added dropwise to microemulsion $AgNO_3$/PP+toluene at 30° C and sonicated for a certain time. The resulting dispersion containing silver sulfide nanoparticles and polypropylene was vacuum evaporated in order to remove the excess of solvent and product was poured on a glass plate to form a polymer film at room temperature. Then by hot pressing at a temperature of fusion of the polymer at a pressure of 10 MPa obtained nanocomposite films.

Ultrasonic processing of materials made in the instrument Sonics Vibramobil VCX 500. The morphology of the nanocomposites and distribution of nanoparticles of silver sulfide in the polymer matrix was studied by atomic force microscopy AFM (INTEGRA PRIMA) and scanning electron microscope (JEOL JSM

14

- 7600F). The optical characteristics of the nanocomposite were investigated by UV spectroscopy Specord250. Thermogravimetric analysis of samples was conducted in a thermogravimetricanalyzer Seiko Exstar 6000 TG/DTA 6300.Nanocomposites samples were heated from 30°C to 600°C with a heating rate of 200C / min in a nitrogen atmosphere.Differential scanning calorimetric analysis of nanocomposites was performed on DSC 6100 (Seiko Instruments Japan) model Differential Scanning Calorimeter (DSC). Samples were placed into aluminum sample pans and experiments were carried out under nitrogen atmosphere with a purge rate of 20 deg/min. Samples were heated from 20°C to 250°C then cooled to 25 °C.

3. RESULTS AND DISCUSSION

The distribution, shape and size of nanoparticles in a polymer matrixof PP/Ag2S nanocomposites, is shown on Figure 1, revealing the electron microscopic images obtained with various contents of silver sulphide nanoparticles (0,0025M, 0,005M, 0,01M). From the SEM images it is clear that with increasing concentration, the size of silver sulphide Ag2S nanoparticles increases. It is assumed that, in the process of the formation of clusters Ag_2S nanoparticles were merged and increased in primary formed centre of crystallization.
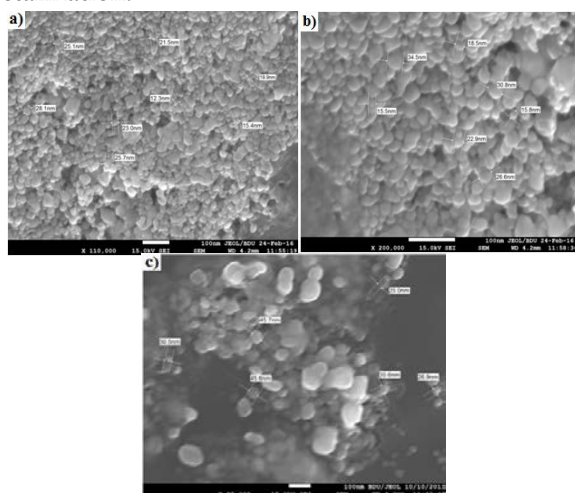
Fig.1. Electron microscope images of nanocomposites based on PP/Ag_2S at various concentrations: a) 0,0025M, b) 0,005M, c) 0,01M PP/Ag_2S.
'

In our opinion it is due to the fact that increasing concentration of the salts solutions the most of the ions Ag+ and S2- spent on coagulation of primary formed Ag_2S nanoparticles but not on the formation of new nuclei. It is found that the shape of nanoparticles is spherical and size of the Ag_2S nanoparticles is approximately 10-50 nm.

SEM study of nanocomposites showed that the distribution of silver sulphide nanoparticles is uniform in polypropylene matrix. Also, experiments show that there is form silver sulphide nanoparticles with small sizes in polypropylene matrix at high concentrations of starting salts.The synthesis technology led to homogeneous distribution of silver sulphide nanoparticles in polypropylene matrix.

The morphology of the nanocomposite PP/Ag_2S and size of distributed Ag_2S nanoparticles was examined with a scanning atomic force microscope (AFM). Figure2 shows the 2D AFM images of the surface nanocomposites PP/Ag_2S, obtained at various concentrations of the starting salts $AgNO_3$ and Na_2S solutions.

AFM study shows that with increasing concentration of the starting salts in the polymer matrix the Ag_2S the particles coagulated. Also it is seems that the size of Ag_2S nanoparticles changes in intervals of 20-60 nm. AFM study also showed that the nanoparticles Ag_2S distributed in the volume of PP matrix, i.e.in pores of the polymer.
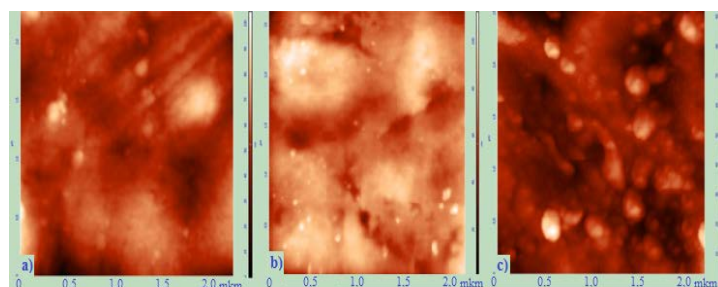
Fig. 2. Atomic force microscopic images of PP/Ag_2S nanocomposites at various concentrations of the starting salts $AgNO_3$ and Na_2S solutions: a) 0,0025M, b) 0,005M, c) 0,01M PP/Ag_2S.

Figure 3 shows the UV-VIS absorption spectra of nanocomposites films of PP/Ag_2S obtained on the various concentrations of Ag_2S.

From Fig.6.seen the absorption intensity increased by increasing concentration of Ag_2S nanoparticles. The peak which corresponds to Ag_2S nanoparticles (445nm) by increasing concentration slightly shifted toward higher wavelength. This is called redshift and indicated the increase of Ag_2S nanoparticles by the increasing of concentrations of starting salts.
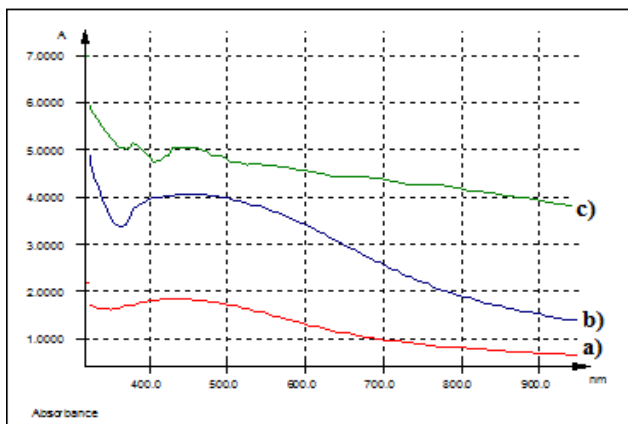
Fig.3. UV spectra nanocomposites PP /Ag$_2$S based on variousconcentrations of Ag$_2$S : a) 0,005 M b) 0,0025 M c) 0,01 M PP/Ag$_2$S.

Thermal behaviour of PP/Ag$_2$S nanocomposites was investigated with two methods. Figure 4. shows TGA curves of the PP and PP/Ag$_2$S nanocomposietes. Note that nanocomposites were prepared using the solutions of salt with three different concentrations. 0,0025M, 0005 M, 0, 01 M PP/Ag2S).
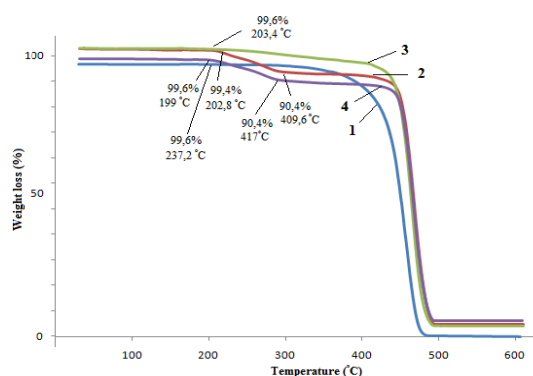
Figure 4. TGA curves of pure polypropylene and nanocomposites on the base PP/Ag$_2$S: 1- PP, 2-0,0025M PP/Ag$_2$S, 3-0,005M PP/Ag$_2$S, 4-0,01M PP/Ag$_2$S.

As it can be seen from the figure, the decomposition of PP occurs at one-stage step. The initial stage of thermal degradation of polypropylene starts at 237,2^0 C and decompose with a continuous weight loss up to 481,110C. 481,11^{0}C. The results of TGA analysis of the samples of pure PP and PP/Ag$_2$S are given in Table 1.

Table 1. Influence of Ag$_2$S nanoparticles weight content on the thermal stability of polypropylene

Samples	PP	PP/Ag$_2$S 0,0025M	PP/Ag$_2$S 0,005M	PP/Ag$_2$S 0,01M
Initial decomposition temperature(°C)	286,6	202,8	203,4	199,5
Half decomposition temperature(°C)	450,68	466,58	462,94	465,9
Final decomposition temperature(°C)	481,11	477,65	489,18	489,11

The formation of Ag$_2$S nanoparticles in polymer matrix influenced the thermal destruction process of nanocomposites. The initial decomposition temperature shifts toward lower temperature. Initial decomposition temperatures of nanocomposites based on Ag$_2$S with 0.0025 M, 0,005 M and 0.01 molar concentrations respectively are 202,8^{0}C, 203,4^{0}C, 199, 5^{0}C. From this result, can be concluded that degeneration of polymer nanocomposites depends on amount of filler.

Thermal properties of those PP/Ag$_2$S composites were evaluated also by means of the differential scanning calorimetry. Melting and crystallization point of DSC curves is shown in figures 5 and 6.
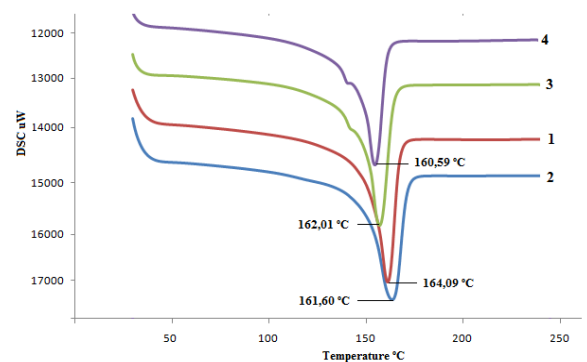
Figure 5. The melting temperature for the PP/Ag$_2$S nanocomposites, derived from DSC analysis 1- PP, 2-0,0025, 3-0,005M, 4-0,01M PP/Ag$_2$S.
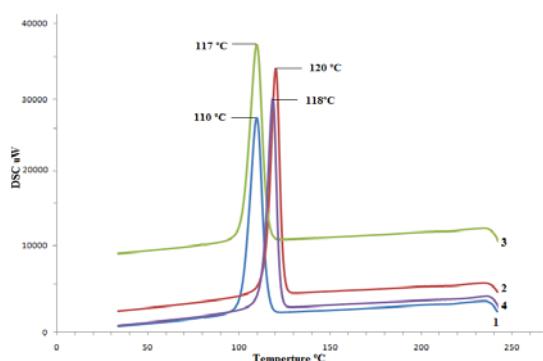
Figure 6. The crystallization temperature for the PP/Ag$_2$S nanocomposites, derived from DSC analysis 1-PP, 2-0,0025M, 3-0,005M, 4-0,01M PP/Ag$_2$S.

Defining the heat of fusion, the degree of crystallinity of the polymer can be calculated which can be investigated by the following relationship:

$$degree\ of\ crstallinity(\%) = \frac{H}{H_0} \cdot 100\%$$

H – melting heat, determined by the area ofpeak responsible for the melting of the polymer, H$_0$ - the heat released at the melting of 100% crystalline polymer, for polypropylene, it is H$_0$ = 207 mJ/mg.

The results of DSC analysis of the samples of pure PP and PP/Ag$_2$S are given in Table2.

Table 2. Data obtained by differential scanning calorimetry for pure PP and PP/Ag$_2$S nanocomposites.

Sample	Meltin temper (°C)	Crystallis temperat (°C)	Meltin enthal (mJ/m	Degree of crystallinit (%)
PP	164	110	92,5	44,68
0,0025M PP/Ag$_2$S	161,6	120	85,1	41,11
0,005M PP/Ag$_2$S	162	117	91,5	44,2
0,01 M PP/Ag$_2$S	160,5	118	79,6	38,45

According to the table, the pure PP melts at 164°C and with the formula (1), the calculated degree of crystallinity of the PP is 44.68%. As it can be seen from the figure 6, the addition of Ag$_2$S fillers does not lead to a significant change in the melting temperature. The degree of crystallinity is increased at 7% weight content of Fe$_3$O$_4$ and then slightly decreases. Furthermore, decreasing the crystallinity degree with increasing of filler concentration in the polymer matrix is due to the destruction of the crystalline phase. Thus, the minimal

decrease in the melting temperatures were observed, which in turn, reduce the degree of crystallization. The reduction of the melting temperature of PP / Ag$_2$S PNC materials may also be related to the presence of defects in matrix after the addition of Ag$_2$S nanoparticles. According to the fact that the lowest melting point of DSC curve correspond to highest concentration of filler one can conclude that, Ag$_2$S nanoparticles accelerate destruction of nanocomposite. In conclusion, addition of filler into polymer matrix subsequently change amorphous and crystalline phase of polymer.

It was found that, addition Ag$_2$S nanoparticles decreases thermal stability of PP/Ag$_2$S nanocomposites. These results are almost consistent with the results obtained by the DSC method.

4. CONCLUSION

In a present paper the structure, morphology and thermal properties of polymer nanocomposites based on PP and Ag2S have been investigated. The distribution, size and shape of Ag$_2$S nanoparticles in polymer matrices were studied by SEM and AFM methods, assumed that with increasing the initial concentration of salt solution, the size of Ag$_2$S nanoparticles increase and led to homogenous distribution ofnanoparticles in the polymer matrix. Also was observed red shifting which also evidenced toincreasing size of nanoparticles. UV spectroscopy indicated that formation of Ag$_2$S nanoparticles in PP matrix affect the destruction process of nanocomposite. Thus, with addition of Ag$_2$S to PP matrix, the small shift in the TGA curve to lower temperature in the initial stage of degradation have been observed. Adding the fillers into the polymer matrix has transformed the formation of amorphous and crystalline parts of composites.

5. REFERRENCES

1. Maharramov A.M., Rramazanov M.A., Hajiyeva F.V. / Chalcogenide Letters, 2016, v. 13, No. 1, p. 35 – 40.
2. Ramazanov M. A., Hajiyeva F. V., Maharramov A. M. & Hasanova U. A. /Journal Ferroelectrics, 2017, VOL. 507, 121–126
3. Maharramov A. M., Ramazanov M. A., Ahmadova A. B., Hajiyeva F. V., Hasanova U. A. / Journal of Nanomaterials and Biostructures Vol. 11, No. 2, April - June 2016, p. 365 – 372

4. Magerramov A.M., Ramazanov M.A., Gadzhieva F.V.and Alieva S.A./j. Surface Engineering and Appleid Electrochemstry, 2011, vol.47, N.5, p.428-432

5. Magerramov A. M., Ramazanov M. A., MustafaevaA.Kh. / Russian Journal of Applied Chemistry, 2010, v.83, №7, p.1324

6. Ramazanov M.A., Hajiyeva F.V., Maharramov A.M. / Ferroelectrics, 2016, v.493, p. 103-109

7. Maharramov A.M., Ramazanov M.A., Nuriyeva S.G., Hajiyeva F.V., Hasanova U.A. / Journal of Optoelectronics and Biomedical Materials Vol. 7, Issue 2, April –June 2015p. 39 -4.

RESISTANCE OF THE SILVER- MODIFIED AND COPPER- MODIFIED ZEOLITE

B.G.SALAMOV**, G.M.EYVAZOVA*, V.I.ORBUKH, N.N.LEBEDEVA, Z.A.AGAMALIEV*

Institute for Physical Problems, Baku State University, Z. Khalilov str.23, Baku, AZ1148

*Nano Centre, BSU, Z. Khalilov str.23, Baku, AZ1148

**Azerbaijan Academy of Science, Institute of Physics, AZ0143 Baku, Azerbaijan

nnlebedeva@gmail.com

The given work presents the results of measuring the temperature dependence of a zeolite modified with both silver and copper. It is established that in the temperature range of 60^0C-90^0C the maximum of this dependence is observed. Its value decreases with increasing frequency, at which the resistance is measured. The explanation of the observed phenomena is based on two assumptions: the first is the presence of a dielectric gap on the surface of the zeolite; the second assumption that the conductivity of the zeolite is realized by local conducting regions separated by a dielectric medium.

1. INTRODUCTION

Clinoptilolite is a high-silica aluminosilicate zeolite. It is represented as a silicon lattice, where part of the Si^{4+} ions is replaced by AL^{3+} ions. The crystal lattice of clinoptilolite is constructed from tetrahedra SiO_4 and AlO_4, where each oxygen atom is at the top of the tetrahedron, being simultaneously the vertex of the neighboring tetrahedron. This arrangement of atoms forms a negatively charged framework containing porous nanocannels of two types with sizes of 0.6×0.4 nm and 0.4×0.4 nm. The off-frame system is positively charged ions (ions of balancing) Na, Ca, Mg, K that compensate for the negative charge of the framework, and also a large number of molecules of H_2O-coordination water [1].

The territory of Azerbaijan is one of the perspective regions for deposits of silica zeolites [2], which are widely used in many fields as ion-exchange substances, adsorbents, molecular sieves, catalysts of chemical reactions. On the basis of X-ray and spectral chemical analysis, we established the belonging of the zeolite investigated by us from the Dashkesan deposite to high-silica zeolites of the clinoptiloline type [3]. The crystal structure belongs to the monoclinic system with parameters $a=17.74A^0$, $b=19.9A^0$ and $c=7.4A^0$, the space group C2/m, $\beta=117^0$.

The conduction current is realized by the motion of mobile ions of the balancing in the anionic framework [4,5]. Hydrated zeolites are also known as proton conductors [6]. Normally, as a rule, it suggests that electronic conduction is not realized in zeolites [7]. In addition, materials such as zeolites have the ability to store energy upon applications of an external electric field [8]. Special electrical properties of the nanopores of the zeolite structure make them good candidate materials in microelectronics [9], gas sensors [10], solar cells [11], functional fillers and composites [12] and plasma light sources with low energy consumption [13].

Thus, it should be noted that the zeolite is actively used as an element of the electrical circuit. However, a systematic study of the zeolite as an electrical circuit element has not been carried out to date. We have in mind the study of the temperature dependencies of the conductivity of a natural zeolite and its modifications. In this study above mentioned measurements for natural, silver- modified and copper- modified zeolites are performed. We choose the silver- modified zeolite because it is widely used in various fields of medicine and biology [14-16], and also because silver and copper are the most highly conductive metals after gold. The most informative characteristics of the electrical circuit element are the measurements of the frequency and temperature dependence of resistance. The conductivity of the zeolite is realized by ion moving in the pores of the zeolite. This conductivity has a hopping character, so it increases exponentially with increasing temperature – exp (-Δ / kT). Real samples consist of chaotically located crystallites separated by voids. Therefore, we

have a question of the temperature dependency of the real zeolite, especially at different frequencies of the external field. To solve this problem, the dependence of the zeolite resistance as a function of temperature at different frequencies was measured in present paper.

2. EXPERIMENTAL

The materials. In this study, a natural zeolite clinoptilolite (ZC) was obtained from two different location: first from the Western part of Turkey (TW) and second from the Dashkesan region of Azerbaijan (AD). The percentage of the elements in the composition both of the zeolite samples (TW and AD) were determined as follows: SiO_2 – 65-72 and 67.84%, Al_2O_3 – 10-12 and 11.36%, CaO – 2.4-3.7 and 2.29%, K_2O – 2.5-3.8 and 2.01%, Fe_2O_3 – 0.7-1.9 and1.19%, MgO – 0.9-1.2 and 0.078%, Na_2O – 0.1-0.5 and 1.25%, P_2O_5 – 0.02-0.03 and 0.11%, MnO – 0.0-0.08 and 0.0%, Cr_2O_3 – 0.0-0.01 and 0.0%, TiO_2 – 0.0 and 0.08%, SO_3 – 0.0 and 0.03%, respectively for the TW and the AD. The percentage values for the same elements in both samples from Turkey and Azerbaijan are very close to each other.

For the measurements, flat plates with thickness of 2.3×10^{-3}m and an area of 1×10^{-4}m^2 were cut from the monoblock of a natural mineral of zeolite. Zeolite powder obtained when cutting the plates was processed in a planetary mill type FRISCH. Phase identification of the samples was done by X-ray powder diffraction (XRD) using diffractometer Rigaki Mini Flex 600 c using a Cu (k_α) radiation. Morphology and elemental compositional analysis were carried out on a scanning electron microscope (SEM, JEOL JSM7600F).

Silver and copper modification of zeolite plates by ion exchange method. The essence of the ion exchange is that the solid material (porous zeolite) absorbs ions (Ag or Cu) from the aqueous solution in exchange for an equivalent amount of the charge exchange ions that are in the pores of the zeolite.

Modification of clinoptilolite with silver implies the following procedure: increasing the number of Na^+ ions in the pores due to displacement of Ca, K, Fe ions from the pores. For this purpose, ion exchange of Na^+ from 0.1M NaCl solution with exchange ions in the pores is carried out. The clinoptilolite plate was immersed into 0.1M NaCl solution for 24 hours. This procedure was necessary in order to facilitate further penetration into the pores due to ion exchange between Ag^+ from the solution and Na^+ in the pore.

Ion exchange between Ag^+ in $AgNO_3$ solution and Na^+ ions in the pores was carried out while the plate was immersed into the 0.02M $AgNO_3$ solution for 24 hours. Then the plate was rinsed with deionized water and dried at 55^0C. Thus a plate of clinoptilolite with Ag^+ ions in the pores was obtained. The silver ions Ag^+ in this sample were chemically redused to silver nanoparticles Ag^0 by placing the plates with silver ions for 40s in 0.1M sodium borohydride ($NaBH_4$) solution. Then the plate was washed in 1l of deionized water and dried at 55^0C.

By the same scheme, the zeolite plate was modified with copper ions: after exchanging exchange ions for Na^+ ions in 0.1 M solution NaCl, the plate was immersed in a 0.02 M solution $[Cu(NO_3)_2]$ for 24 hours, then it was washed in deionized water and dried at 55^0C.To restore Cu^+ ions in the pores to copper nanoparticles, a solution of sodium borohydride was prepared. The plate of clinoptilolite with copper ions in the pores was immersed for 40 s. in 0.1 M of this solution. After that, the plate was washed in deionized water and dried at 55^0C.

Thus, we had the following types of the samples:

- natural clinoptilolite modified with silver ions;
- natural clinoptilolite modified with silver nanoparticles;
- natural clinoptilolite modified with copper ions;
- natural clinoptilolite modified with copper nanoparticles.

The electrical properties of the samples were measured by impedance spectroscopy [17,18].For the measurements, the samples were placed in a cell between two polish planar metallic electrodes. ZC plate is sandwiched in a cell. The cell connected to the LRC (impedance, resistance and capacitance) impedance meter E7-20 (frequency range 200Hz-1MHz). The measurements were taken in the temperature range of 20^0C -120^0C, atmospheric pressure and air humidity 0.85%.

3. RESULTS AND DISCUSSION

The temperature dependence of the resistance at different frequencies was measured for samples modified with silver and copper ions and nanoparticles . Fig. 1 and 2 show the results of measurements at fixed frequencies in the range of 120 Hz – 5 kHz.

20

The same character of the dependence of the resistance on temperature is observed in Figs. 1 and 2: 1) the resistance increases with increasing temperature, and when the temperature reaches 60ºC - 80ºC, after an insignificant decrease, practically does not change; 2) there is no temperature dependence at high frequencies (5 kHz).

To describe the temperature dependence of the resistance of zeolite, modified with copper (or silver), we consider the possible mechanisms of such dependence. The conductivity in pores is realized by ions localized on their walls. The presented graphs of the temperature dependence of the zeolite resistance for different frequencies shows that the resistance, as a whole, grows with increasing temperature, and a maximum is observed at low frequencies. To explain the observed dependencies, we shall rely on the results of [19], in which the frequency dependence of the zeolite resistance $R(\omega)$ was explain by taking into account the dielectric gap on the zeolite surface. In this paper we obtained the following formula:

$$R(\omega) = R_0 \left\{ \left(1 + \frac{C}{C_s} \right)^2 + \frac{1}{(\omega C_s R_0)^2} \right\} \qquad (1)$$
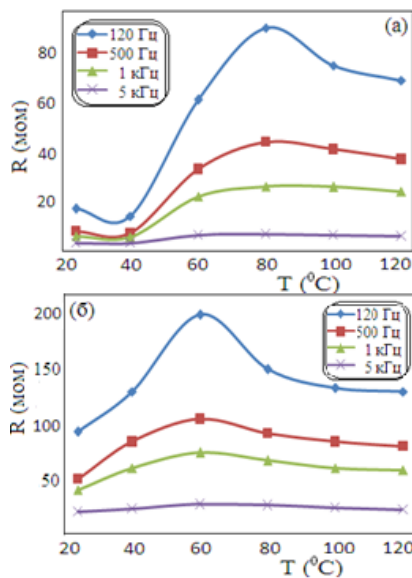
Figure 1 The temperature dependence of the resistance of zeolite, modified with silver ions (a) and nanoparticles (b)
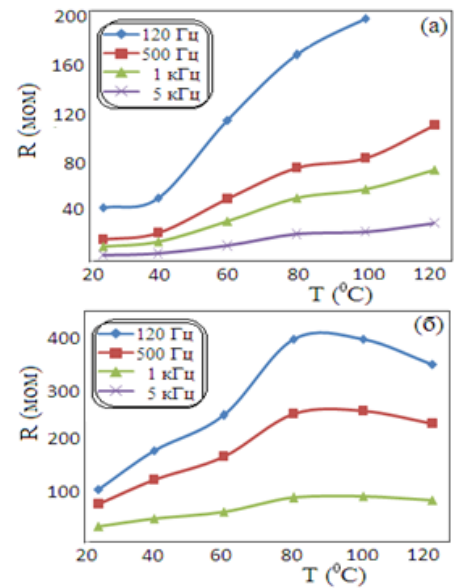
Figure 1 The temperature dependence of the resistance of zeolite, modified with copper ions (a) and nanoparticles (b)

Here, R_o – bulk resistance of zeolite, C – bulk capacitance, C_s – the capacitance of the dielectric gap on the zeolite surface, ω - the frequency of the external electric field. Since the graphs of the temperature dependencies for different frequencies are different, we consider (1) in the low - frequency region, where the resistance depends on the frequency. At low frequencies, when $\omega C_s R_o < 1$, the first term in the curly brackets of the form (1) can be neglected. Then (1) can be rewritten as (taking into account that $R = L\sigma/S$);

$$R(\omega) = \frac{S\sigma}{\omega^2 C_s^2 L} \qquad (2)$$

There, L – zeolite plate thickness, S – surface area, C_s - capacitance of the dielectric layer on the zeolite surface. It follows from this formula, that at low frequencies the dependence of the resistance on the frequency is proportional to the bulk conductivity. Such an unusual conclusion has a simple explanation. At low frequencies, the Maxwellian time of displacement of the external electric field from the conducting volume to the dielectric gap is much less than the period of the external field $(\omega C_s R_o < 1)$. Under these conditions, the resistance of the sample - dielectric gap system also increases with increasing conductivity, since most of the period of the internal field is in the dielectric gap, and not in the

21

conducting volume. To explain the behavior of the temperature dependence of the resistance at different frequencies, it is sufficient to assume that the conductivity of the zeolite is carried out by isolated conductive regions immersed in a dielectric medium.

We use the formula for the dielectric constant of a dielectric medium in which the conducting regions are located [20],

$$\varepsilon_m = \varepsilon_1 + C \frac{3\varepsilon_1 (\varepsilon_2 - \varepsilon_1)}{\varepsilon_2 + 2\varepsilon_1} \qquad (3)$$

Here, ε_m - is the dielectric constant of the mixture, index 1 refers to the medium, index 2 – to local regions with a different dielectric permittivity, C - is the density of these regions.

We consider the model when the real part of the dielectric constant is the same for the medium and the local regions, and the imaginary part is different from zero only for the local regions. Then (3) takes the form;

$$\sigma(\omega) = 9\varepsilon^2 c \frac{\sigma_0 \varepsilon_0^2 \omega^2}{9\varepsilon^2 \varepsilon_0^2 \omega^2 + \sigma_0^2} \qquad (4)$$

Here, σ - is the average conductivity of the system, σ_o - conductivity of the local conducting region, ε - the dielectric constant of both the conductive isolated regions and the dielectric regions separating them, ε_o - the dielectric constant, C – the ratio of the volume of the sample occupied by the conducting regions to the total volume. Substituting (4) into (2), we obtain

$$R(\omega) = C \frac{9\varepsilon^2 \varepsilon_0^2 S}{C_s L} \frac{\sigma_0}{9\varepsilon^2 \varepsilon_0^2 \omega^2 + \sigma_0^2} \qquad (5)$$

$R(\omega)$ has a maximum as a function of σ_o. To find it, we equate the derivative of $R(\omega)$ with ω to zero. As a result, we obtain a maximum at:

$$\sigma_o^{\ max} = 3\varepsilon_o \varepsilon \omega \qquad (6)$$

is equal to

$$R(\omega)^{max} = \frac{3\varepsilon\varepsilon_0 S}{2C_s L\omega} \qquad (7)$$

This result explains the peaks in Fig. 1(a,b) and Fig. 2(b). Indeed, as the frequency increases, the value of the resistance maximum decreases according to formula (7). The value, depending on the temperature, in form (8) is:

$$\sigma_0 = \sigma_\infty \exp(-\frac{\Delta E}{kT}) \qquad (8)$$

Here, σ_∞ is a weakly temperature - dependent pre-exponential factor proportional to the carrier density, ΔE is the activation energy of the hopping conductivity, k – the Boltzmann constant, T – the absolute temperature. From (6) and (8) we obtain the expression for the temperature of the resistance maximum:

$$T_{max} = \frac{\Delta E}{k \ln\left(\dfrac{\sigma_\infty}{3\varepsilon\varepsilon_0\omega}\right)}$$

(9)

4. CONCLUSION

In the present study, a maximum in the temperature dependence of the resistance of the zeolite was found. With increasing frequency of the external field the value of maximum decreases, and its half-width increases. The explanation given by us is based on two propositions. First, there is a dielectric gap on the surface of the zeolite, and second, conductivity is realized by local conducting regions. The presence of a dielectric gap leads to a frequency dependence of the resistance, since the electric field is pumped from the zeolite volume into the gap. Because of this, the measured resistance is proportional to the bulk conductivity at low frequencies. The fact is that the greater the bulk conductivity, the smaller the Maxwellian time and the greater part of electric field period is concentrated on the electric gap, i.e. , the measured resistance increases. The presence of a peak in the temperature dependence of the resistance is explained by the presence of local conducting regions, the resistance of which has a maximum as a function of temperature. The increase of resistance in samples with nanoparticles is associated with a decrease of the number of mobile ions from which nanoparticles are formed. The absence of the peak of temperature dependence of the copper-modified zeolite is due to the fact that the temperature maximum is outside the temperature range in which the measurements were carried out . And the peak position does not change with increasing frequency (due to the weak logarithmic dependence on frequency).

5. REFERENCES

1. Gottardi G. et al. Berlin: Springer-Verlag; 1985, p. 409.
2. Amirov CE. Seoliti Azerbaijana, Baku: Elm; 2004, p.22.
3. Kuliyeva TZ. et al. /J. Fizika, 2009, v.15, p.43-45.
4. Kelemen G. et al. /J. of Materials Science, 1992, v.27, p.6036-6040.
5. Goryainov SV. et al. /Physica B: Condensed Matter, 2007, v.390, p.356-365.
6. John CMc. Et al. /Chemistry of Materials, 2008, v.20, p.5122-5124.
7. Rutter MD. et al. /Chemical Physics Letters, 2000, v.331, p.189-195.
8. Praveena K. et al. / nternational J. of Emerging Technology and Advanced Engineering, 2013, v.3, p.363-372.
9. Alvaro M. et al. /Chemistry of Materials , 2006, v.18, p.26-33.
10. Sahner K. et al. /J.Solid State Ionics, 2008, v.179, p. 2416-2423.
11. Alienzar P. et al. /Chem. Phys.Chem., 2007, v.8 , p.1115-1119.
12. Suresh K. et al. /J. Polymer Research., 2010, v.17, p.135-142.
13. Koseoglu K. et al. /Japenese, J.of Applied Physics, 2014, v.53, 086203.
14. Silver S. /FEMS Microbiology Reviews, 2003, v.27, p. 341-353.
15. Tiscomia I. et al. /J. Physical Chemistry , 2007, v.111, p.4702-4709.
16. Dhermendra Tivari K. et al. /World Applied Scienses Journal, 2008, v.3, p.417-433.
17. Macdonald JR. /Annals of Biomedical Ingineering, 1992, v.20, p.289-305.
18. Minbrik S. et al. /J. Optoelectronics and Advanced Mat., 2007, v.9, p. 872-874.
19. Orbukh VI et al. /Transactions ANAS Phys. Astron., 2015, v.35, p.51-54.
20. Landau LD et al. Electrodinamika sploshnix sred, Moscva: Nauka, 1982, p.632.

PHOTO- AND GAS SENSITIVITY OF HETEROJUNCTIONS *c*-Si/*porous*-Si/CdS

H.M. MAMEDOV[a]*, M.MURADOV[a], M.JAFAROV[a], Z.KONYA[b], A.KUKOVECZ[b], K.KORDAS[c], S.I. SHAH[d], V.J.MAMEDOVA[a], K.M.AHMEDOVA[a], V.U.MAMEDOV[a], E.A.KHANMAMEDOVA[a]

[a] Baku State University, Z.Khalilov str., 23, Baku, Azerbaijan, Az1148
[b] University of Szeged, Dugonicstér 13, Szeged, Hungary, Szeged 6720
[c] Microelectronics Research Unit, University of Oulu, P.O.Box4500,90570, Oulu, Finland
[d]University of Delaware 208 DuPont Hall Newark, USA, DE 19716

Heterojunctions of *c*-Si/*porous*-Si/CdS were produced, by the methods of electrochemical deposition (CdS) and anodization (*porous*-Si). Electrical, photoelectrical and gas sensing characteristics of heterojunctions were studied, depending on the crystallite size of CdS and pores size of Si. The optimal size of pores (10 nm) was defined which provides the maximum efficiency (7.71%) of heterojunctions.

1. INTRODUCTION

Thin film heterojunctions of p(n)-Si/CdS are promising candidates for solar cell application [1-3]. Since, application of wide-gap semiconductors as optical window in silicon-based heterojunctions, to some extent, allows minimizing the free charge losses due to surface recombination. However, significant difference in the lattice constants of silicon and CdS (about 7%) stimulates the formation of surface states at interface. Application of the ternary ($Zn_{1-x}Cd_xS$) and even quaternary ($Zn_{1-x}Cd_xS_{1-y}Se_y$) solutions of A^2B^6 type semiconductors, as reported by us [4, 5], has succeeded in reducing the lattice mismatch and concentration of surface states at interface, but it has not been possible to achieve sufficiently value of efficiency due to the large value of silicon refractive index. The use of porous silicon as an intermediate layer between the absorber and buffer, allows not only solving problems with lattice mismatches, and surface reflections related to refractive index of silicon, as reported by authors [6-10].

CdS thin films have been prepared by a variety of techniques [11-15]. However, these techniques are plagued with their own drawbacks and difficulties. Among these techniques, electrochemical deposition yields films with different structure and surface morphology by a relatively simpler process. Electrochemical deposition that used in this work is generally less expensive than the capital-intensive physical methods [16-20].

2. EXPERIMENT

To manufacture the heterojunctions, p-type *c*-Si wafers (2.5 Ohm·cm resistivity and 0.2 ÷ 0.3 mm thickness) of (100) orientation were used as a substrate. Before anodization, the surface of the *c*-Si substrates were etched in an aqueous solution of HF and further washed in distilled water (at temperature of 80°C) and ethyl alcohol and then dried in air. The anodization of *c*-Si substrate surface was carried out in Teflon chamber with Pt cathode. HF: ethanol solution (1:1) were used for the porous silicon formation. The anodization voltage, current density and anodization time were 30V, 40-70 mA/cm^2 and 30–1800 sec, correspondingly. Depending on the anodization current and time porous-Si with porous size of 7 – 50 nm were prepared on the surface of *c*-Si.

In order to fabricate the heterojunctions, an ohmic In electrode, in reticulose form was evaporated on the CdS films with an area of ~0.82-1cm^2. An ohmic contact was performed on the side of *c*-Si wafers by evaporating an Al electrode.

3. RESULTS AND DISCUSSION

The morphology of PS was investigated using SEM (Figure 1). SEM data indicate that the increase of anodization current density leads to the increase of the resulting pore size and a significant surface flattening between the pores.

After the PS layer formation, samples was immersed into ethyl alcohol, dried in air and placed into the electrochemical bath for the deposition of nanostructure CdS films. Electrodeposition of the CdS films onto the *c*-Si/*porous*-Si (with porous size of 7.4; 10 and 30 nm)

24

substrates was carried out at temperature of 80°C from aqueous solution containing cadmium (CdCl$_2$) and sodium (Na$_2$S$_2$O$_3$) salts. Cyclic voltammetry was used to monitor the electrochemical reactions in solutions of CdCl$_2$ and Na$_2$S$_2$O$_3$, then in their combined solution of the same concentration and pH. The cyclic voltammograms was scanned in the potential range 1.2 V to –1.2 V versus graphite (or Ag/AgCl) electrodes. Depending on the deposition time, substrate pores size and the individual system, CdS films (with thickness up to 0.2 ÷ 0.6 μm) with different morphology were obtained from a solution. In order to achieve a more direct insight into the surface structural features of the films, SEM imaging had been performed. SEM images of thin films CdS deposited at potential of 0.82 V onto the *c*-Si/PS (with pores size of 7.4; 10 and 30 nm) are shown in Figure 2. As seen from figure, the size of crystallites of the CdS films can be controlled by selecting the pores size of silicon.

The films deposited onto the substrates with pores size 7.4 nm shows micro-texture structure. The grain sizes were in the range from ~20 to 70 μm. As seen from Figure 2c, when Si with pores size of 10 nm is used as substrate, the size of the nano-grains gets reduced due to controlled process of nucleation and nano-size grains are uniformly distributed at the surface.

Size of particles, as determined by SEM, is found as 80-190 nm. As seen from SEM images, CdS films shows nano-grain texture, with increasing the pores size from 10 to 30 nm (Figure 2 b). The size of the grains was different from each other, indicating irregular growth rate of the grains.

Photo- and gas sensitivity of heterojunctions were studied depending on the crystallite and pores size. Current-voltage characteristics (*J-V*) of heterojunctions show rectification.

It is established that rectification factor values and current passage mechanism through junction region depends on the pores and crystallite size.

The pass direction corresponds to positive polarity of the external bias on the *c*-Si layers. Rectification increases from 180 up to 1100, with increasing the pores size from 7.4 to 10 nm.

Further increase in pore sizes leads to sharp decrease of rectification (~12÷15). It is assumed that the change in rectification factor value depending on the pore size is due to the oxygen or nitrogen molecules, because in order to remove excess water from pores and films,

heterojunctions were dried in air, just after the deposition (as-deposited heterojunctions).
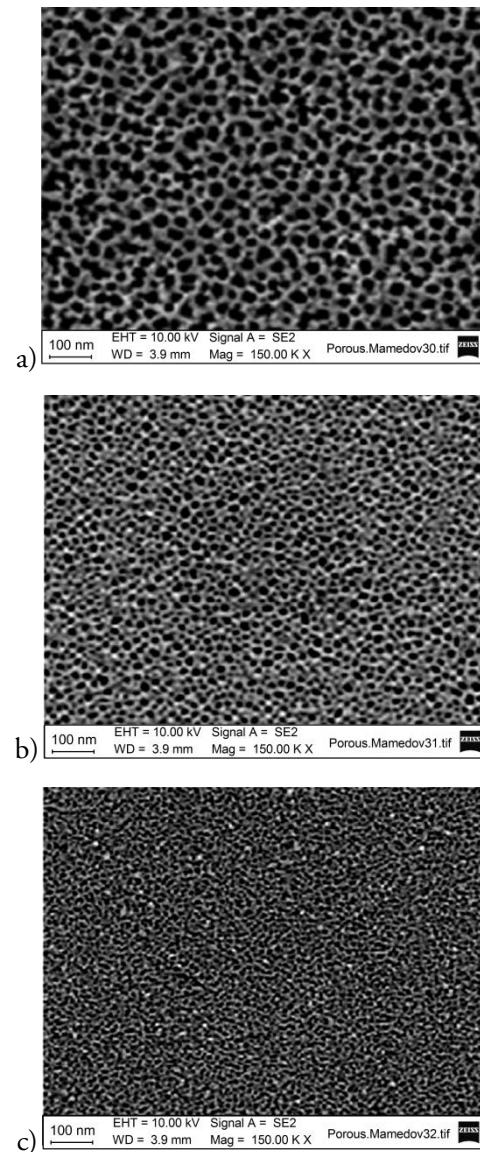
Figure 1. SEM images of porous silicon prepared at different regimes of anodization: (a) 30V; 70 mA/cm^2; 1800 sec; (b) 30V; 55 mA/cm^2; 1800 sec; (c) 30 V; 40 mA/cm^2; 400 sec.

In this case, adsorbed oxygen or nitrogen molecules to the silicon pores creates the acceptor states in junction region and thus increase recombination acts. It is established that the degree of adsorption depends on pores size. To confirm this fact, heterojunctions were heated in vacuum at 50-70°C and *J-V* characteristics were taken in vacuum. It is established that rectification in heterojunctions with pore size of 7.4 and 10 nm remained almost unchanged.
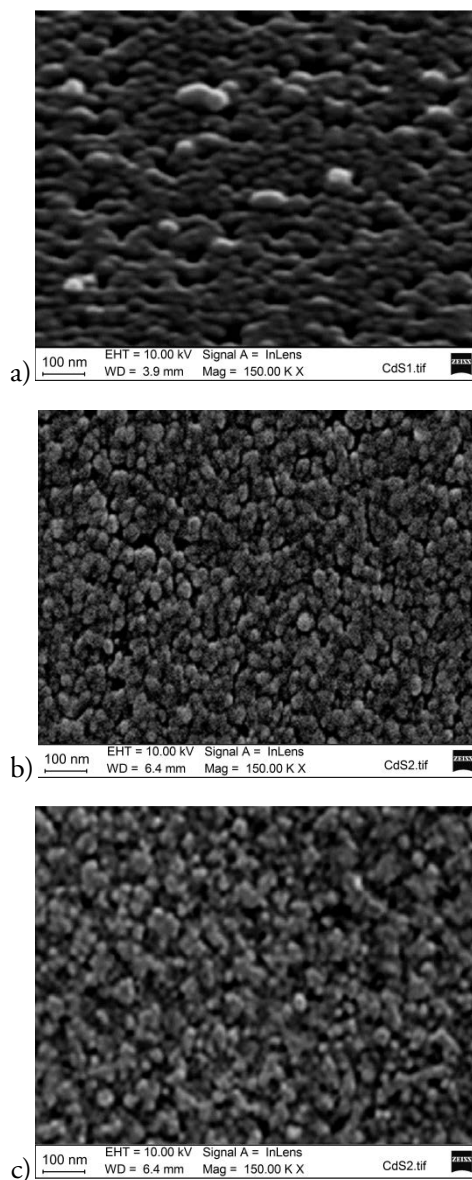
Figure 2. SEM images of electrdeposited films CdS: (a) p-Si/7.4 nm *porous*-Si/CdS; (b) p-Si/10 nm *porous*-Si/CdS; (c) p-Si/30 nm *porous*-Si/CdS.

But the rectification in heterojunctions with a pore size of 30 nm increases sharply (980-1000). In our opinion, this is due to desorption of oxygen or nitrogen molecules. To prove this, we carried out additional experiments on these heterojunctions. Direct current at U= 1 V was measured in air with different concentrations. Direct current in heterojunctions with 10 nm not changed, and in heterojunctions with 30 nm decreased with increasing air concentration (Figure 3 a).

The dependence of direct current at U=1 V for heterojunctions with pores size of 7.4; 10 and 30 nm, on the concentration of various gases (oxygen, nitrogen, methane and ethanol vapor) have been investigated. As

seen from Figure 3 (b) and (c), the direct current decreases at insignificant change of the gas concentration. It is suggested that heterojunctions with pore sizes of 30 nm can be used as gas sensors.
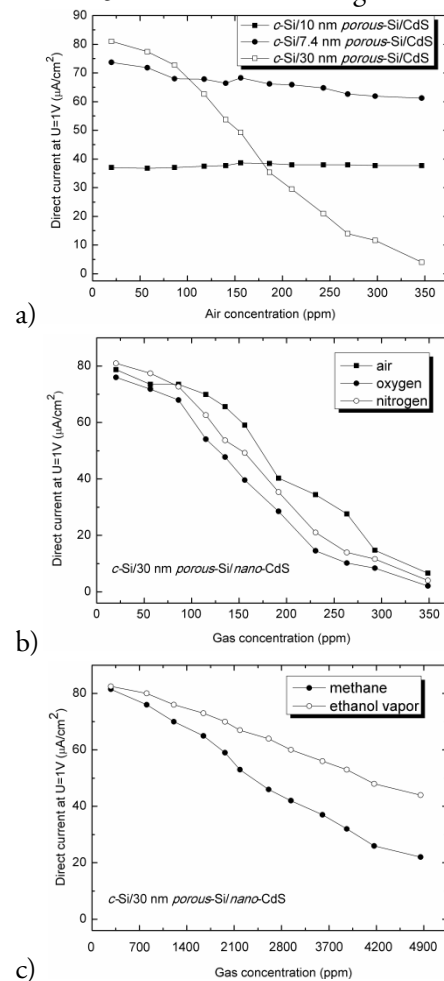
Figure 3. Dependence of direct current at U=1 V on the air concentration (a) for heterojunctions p-Si/*porous*-Si/CdS with different pores size, and on the concentration (b, c) of different gas for heterojunctions with 30 nm pores size.

Experiments carried out in various atmospheres on heterojunctions with pores size of 7.4 nm, showed insignificant changes of current and junctions with pores size of 10 nm do not showed any change of direct current, i.e. they have stable parameters. This fact testifies that heterojunctions with pores size of 7.4 and 10 nm can be used for manufacturing of solar cells.

All investigated samples under standard test conditions demonstrated photovoltaic performances under AM1.5 illumination (W=100 mW/cm^2), which sign of open circuit photo-voltage (U_{oc}) does not change in all region of photosensitivity. However, the maximum values of U_{oc} and J_{sc} non-monotonically dependent on the pores size of Si. The maximum values

of U_{oc} and J_{sc} were observed in heterojunctions with pore sizes of 10-17 nm (Figure 4).
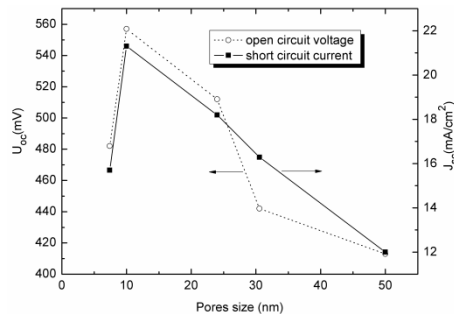
Figure 4. Dependence of open circuit voltage and short circuit current density in heterojunctions of *c*-Si/*porous*-Si/CdS.

In order to explain the reason of this, we investigated the spectral distribution of photocurrent (J_{ph}) depending on the pores size of silicon and morphology of CdS films, in a wavelength range of 300÷1300 nm (Figure 5). It is established that the profile of photocurrent spectrum depends on the pore size and morphology of CdS films. Short wavelength peak for heterojunctions with a pore size of 7.4 nm, is observed at 510 nm, which corresponds to the band gap of CdS films. The films deposited onto the silicon with pore size of 7.4 nm shows micro-structural morphology, as demonstrated by SEM images.
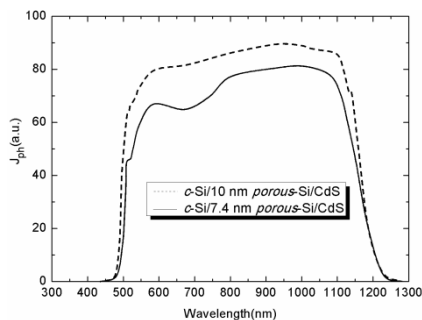
Figure 5. Spectral distribution of photocurrent in heterojunctions depending on the pores size in Si.

However, long-wavelength peak of spectrum at 1125 nm is due to the direct interband transitions in *c*-Si. It can be seen from Figure 5, that heterojunctions demonstrate good photo-response in the wavelength range of 512 ÷ 623 nm, which is not observed by us in heterojunctions of c-Si/A_2B_6 [4, 5]. It is assumed that this is due to light absorption in porous silicon. With increasing pores size until 10 nm, shift of peak at 510 nm to the short wavelength region of spectrum is observed, which associated by us with the nano-structural properties of CdS films [21, 22], i.e. band gap

increasing with decrease of crystallite sizes in films. However, an increase of the optical path of light in nano-structured films leads to increase of degree of the light absorption, therefore, heterojunctions with pore sizes of 10 nm, shows greater efficiency compared heterojunctions with pore sizes of 7.4 nm (Table 1).

Table 1. Electrical and photoelectrical parameteres of heterojunctions depending on the pores size in Si

Samples	Ideality factor	Rectification factor	U_{oc} (mV)	J_{sc} (mA/cm²)	FF	η, %
c-Si/7.4nm *porous*-Si/CdS	1.68	180	482	15.7	0.53	4.01
c-Si/10nm *porous*-Si/CdS	1.4	1100	557	21.3	0.65	7.71

4. CONCLUSION

It has been established that regulating size of pores in the silicon can be specifically control the morphology of CdS films. Heterojunctions with pore sizes of 30 nm can be used as some of the gas sensors. But heterojunctions with pores size of 10 nm, can be used as solar cells with an efficiency of 7.71%.

5. REFERENCES

1. Suda T., Kuroyanagi A., / Journal of Crystal Growth, 1983, v. 61, p. 494-498.
2. Hayashi T., Nishikura T., Nishimura K., Ema Y/ Japanese Journal of Applied Physics, 1989, v.28, p.1174-1178
3. Katiyar A.K., et al. / ACS Appl. Mater. Interfaces, 2015, v. 7, p.23445–23453.
4. Abdinov A., Mamedov H., Hasanov H., Amirova S /Thin Solid Films, 2005, v. 480-481, p.388-391.
5. Abdinov A., Mamedov H., Amirova S./ Thin Solid Films, 2006, v.511-512, p.140-142.
6. Foll H., Christophersen M., Carstensen J., Hasse G /Materials Science and Engineering R, 2002, v.280 p. 1–49.
7. Granitzer P., Rumpf K./Materials. 2010, v.3, p.943-998; doi:10.3390/ma3020943.
8.Korotcenkov G. (ed.), Porous Silicon: From Formation to Application, v. 3: Microelectronics, Optoelectronics and Energy Technology Applications, Taylor and Francis Group, CRC Press, Boca Raton, USA, 2016.

9. Yerokhov V. Y., Melnik I. I./Renewable and Sustainable Energy Rev., 1999, v.3, p.291-322.

10. Ramizy A., et al./ Appl. Surf. Science, 2011, v.257, p. 6112-6117.

11. Oliva A.I. et al./ Thin Solid Films, 2001, v.391, p. 28-35.

12. Ashour A. et al./Thin Solid Films, 1995, v.269, p. 117- 120.

13. Ashoour A./ Turk. J. Phys., 2003, v. 27, p.551-558.

14. Keitoku S.,et al./ Japan J. Appl. Phys., 1995, v.34, p. 138-141.

15. Boieriu P. /Journal of Electronic Materials, 2000, v.29, p. 718–722.

16. Abdinov A., Mamedov H., Amirova S. /Japan J. Appl. Phys., 2007, v.46, p. 7359-7362.

17. Abdinov A., Mamedov H., et al./Thin Solid Films, 2005, v.480-481, p.388-391.

18. Abdinov A., Mamedov H., Amirova S./Thin Solid Films, 2006, v.511-512, p.140-142.

19. Mamedov H., et al./ Journal of Solar Energy Engineering, 2014, v.136, p.044503-1-4.

20. Mamedov H., et al./ Journal of Optoelectronics and Advanced Materials, 2015, v.17, p. 67 – 73.

21. Mahdi M.A./ Thin Solid Films, 2012, v.520, p.3477–3484.

22. Chen M., et al./J. Nanosci. Nanotechnol., 2009, v. 9, p. 1505-1508.

LUMINESCENCE PROPERTIES OF   ZnS:Co NANOPARTICLES

M.JAFAROV[a], I.HASANOV[b], E.A.KHANMAMEDOVA[b]

[a]Baku State University, Z.Khalilov str., 23, Baku, Azerbaijan, Az1148
[b]ANAS, Institute of Physics, Istiqlaliyyat str.30, Baku, Az1001

An aqueous solution method has been developed for synthesizing size-controlled ZnS:Co nanocrystals with a relatively narrow size distribution. The nanocrystal samples were characterized by UV-Vis absorption spectra and photoluminescence spectra. We prepared narrow size distribution particles under different synthesis conditions. The effect of manganese concentration on the photoluminescence properties was investigated. Luminescence intensity in different excitation wavelength correlates with different size of ZnS:Co nanocrystals on luminescence spectra. We found that by narrowing the size distribution and doping concentration, ZnS:Co samples can be prepared with high luminescence intensity.

Keywords: aqueous solution, nanoscale materials, nanoparticles, luminescence

1. INTRODUCTION

Nanoscale materials researches have stimulated great interest owing to their importance in basic scientific research and potential technological applications. The synthesis of doped nanocrystals has become a major field of recent researches. ZnS:Co nanocrystals have been mainly studied due to the luminescence of the Co^{2+} ions inside the ZnS host. This is due to the fact that Co^{2+} ions provide good traps for the excited electrons, which give rise to their potential use in nonlinear optics, optoelectronic devices, solar cells, photodetectors and light-emitting diodes [1–3]. This paper presents some interesting results obtained on the synthesis of ZnS:Co nanocrystals by the aqueous solution method with controllable and narrow size distribution. We treat the effect of Co doping on the luminescence properties of ZnS nanoparticles. Also, we consider the effect of various synthesizing conditions on the narrow size distribution of the ZnS:Co particles and the luminescence intensity.

Aqueous solutions of zink chloride, cobalt chloride and the capping agent thioglycerol (TG) of high (0.1 M) and low (0.01 M) concentrations are prepared in ethanol. The pH was adjusted to about 2–10 by adding appropriate amounts of NaOH, before adding TG. Sodium sulfide dissolved in distilled water was added dropwise to the mixture for 5 min. The total reaction time was about 2 h. Nitrogen gas was used for deoxygenating the reaction vessel. The temperature in different experiments ranged between 30^0C and 70^0C. In high temperature experiments, the synthesis vessel was heated in the bath. The synthesis solution was washed with acetone to get rid of unreacted ions remaining outside the clusters and then was centrifuged. Finally, the precipitate was air-dried to get a powder of ZnS:Co nanoparticles. The optical absorption spectra of ZnS:Co nanocrystallites dispersed in ethanol were recovered using a UV-Vis spectrophotometer (Cary 100). The luminescence spectra were recorded on a LF-5 Perkin Elmer spectrometer with the excitation wavelengths of about 370 nm to excite the ZnS:Co nanocrystals. Deposited films were kept "as it were" for the other characterization like XRD, AFM and XRF. Thickness of the films was measured by gravity method. Thickness for ZnS, ZnS:Co films was varied from 84 – 85.26 nm.

2. RESULTS AND DISCUSSION

Fig. 1 shows the XRD patterns of ZnS:Co thin films deposited at fixed pH value and temperature of 70°C. The XRD peaks appear at 33.20°, 47.32°, 56.36° and 69.4° in the pure ZnS film corresponding to the diffraction from (200), (220), (311), (400) planes respectively of the cubic phase of ZnS. Results are very much closer to the value of JCPDS card file 05-0566. Same diffraction peaks are also observed in the ZnS:Co films except in the 0.05M CoO_3 doped film (ZnS:Co), where the (400) plane is absent. Thus all the deposited films are polycrystalline in nature. From the XRD spectra it is clear that the intensity of (200) plane in all the films is higher than that of the other peaks which indicates that the orientation of the grain growth is along (200) plane.

Atomic force microscopy (AFM) is one of the effective ways for the surface analysis of thin films due to its high resolution and powerful analysis software. The ZnS and ZnS:Co thin films were morphologically characterized using AFM technique. Fig. 2 shows the

29

image of ZnS:Co film in scanned area of 5 × 5 and 10 × 10 μm². In both the films the surface is rough and fully covered in the substrate. Clusters of particles are observed over the surface in undoped ZnS film. While formation of unregulated grains of different sizes are observed clearly with pinhole free in ZnS:Co film.
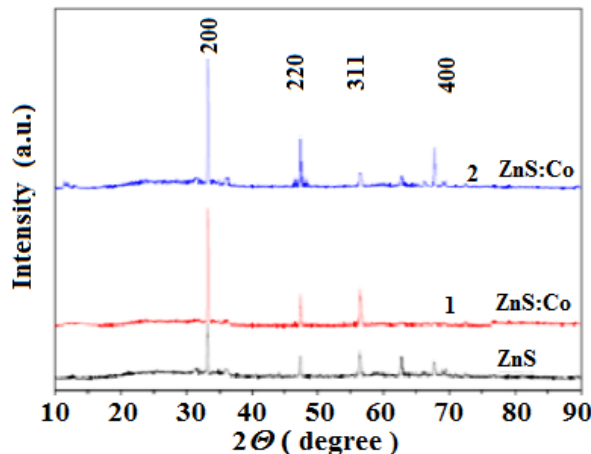
Fig. 1. XRD spectra of ZnS:Co undoped nanocrystals, 5% (1) and 10% (2) doping nanocrystals (pH-4)
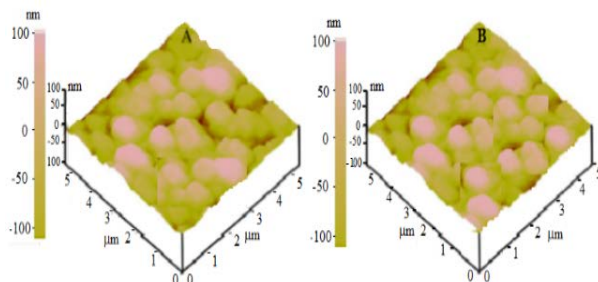
Fig.2. AFM images of (a) ZnS and (b) ZnS:Co films

Optical absorption of Zns and ZnS:Co films have been studied in the wave length range 340-800 nm. Optical absorption studies of semiconducting materials give some information related to band structure. Optical absorption spectra of typical undoped ZnS:Co thin films have been shown in Fig. 3. At higher wavelength i.e. at lower energy side, absorption is low towards visible region.

However, an increase of absorption is seen in lower wave length (higher energy) side for both types of films. Higher absorbance has been observed in Co doped ZnS films. This may due to the presence of extra states created by Co impurity in the doped films that absorbs more photon energy than that of the undoped film.

These activities in the host material define the luminescence efficiency and can produce a narrowing or broadening of the bandwidth of the spectra. As shown in all figures, we have three peaks that can

correspond to band edge, shallow traps, and deep traps. Figure 4 shows the PL spectra and absorption spectra of a series of samples with different doping concentration.
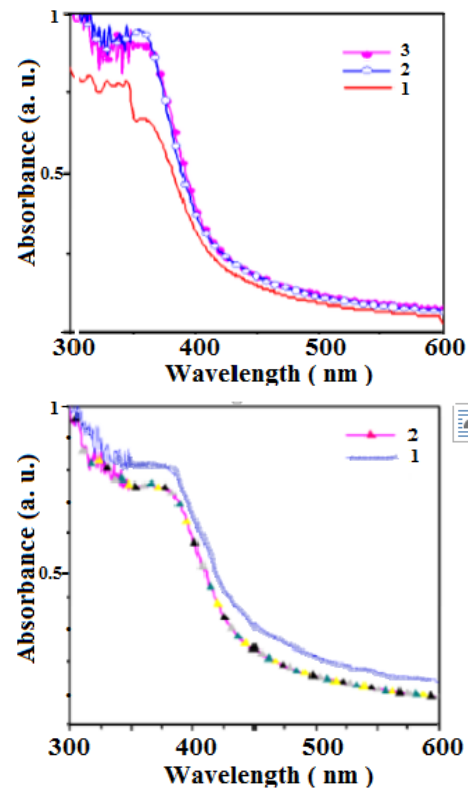
Fig. 3. Absorbance spectra of ZnS:Co undoped nanocrystals (1), 5% (2) and 10% (3) doping nanocrystals (pH-4) (a) and the luminescence intensity decreases with increasing pH (b):1-2, 2-8

The PL spectra (Fig. 4a) of the nanocrystal samples show three peaks, at 444, 478, and 530 nm, which are attributed to the band edge, shallow and deep traps, respectively. We see that undoped nanocrystals have a narrower size distribution than the 5% and 10% doping nanocrystals.

Therefore they have the highest emission intensity. But we expected doping Co ions to produce better luminescence spectra. The impurity concentrations generally are low in view of the fact that at higher concentration the efficiency of the luminescence process usually decreases (concentration quenching). It may be that, at high concentration, there is the broad size distribution of nanocrystals and broad emission wavelength, and as a result, low luminescence intensity.

As we show in Fig. 4,b the luminescence intensity decreases with increasing pH. The absorption spectra in pH 4 have sharper excitonic peaks than pH 2 and 10, respectively. Moreover, it was found that CoS can create an acidic synthesis solution which produces

30

radiative recombination centers in the ZnS host material. We prepared ZnS:Co nanocrystals at a high precursor concentration with 0.1 M.
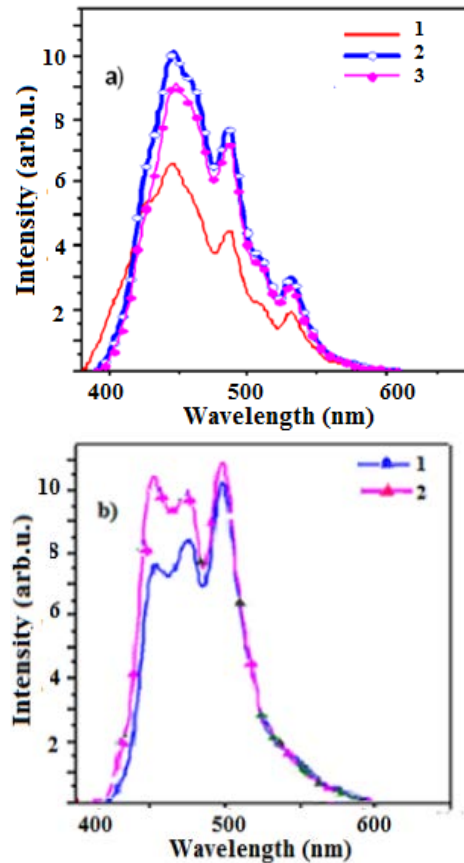
Fig. 4. Luminescence spectra of ZnS:Co undoped nanocrystals (1), 5% (2) and 10% (3) doping nanocrystals

(pH-4) (a) and the luminescence intensity decreaseswith increasing pH (b):1-2, 2-8

3. CONCLUSION

It means that doping of nanocrystals occurs completely in high precursor concentration. Also, we investigated the optimize conditions for thebest luminescence with different excitation wavelengths and doping concentrations there is a narrowing of the excitonic absorption peak at 350 nm. We excited sample *K* with three excitation wavelengths. There is the best luminescence for 360 nm excitation which is near to band edge wavelength. Two other excited emissions related tothe sizes of other nanoparticles were distributed in this sample. We find a red-shift of the band edge emission by varying the excited wavelength. But we have abroad peak at 465 nm in all of them that is related to the incorporation of non radiative and radiative recombination.

4. REFERENCES

1. Bhargava R.N., Gallagher D. and Welker T./ J. Lumin., 1994, v. 60(61) p. 275-279
2. Lu H. and Chu S.Y.S./ J. Cryst. Growth., 2004, v. 265, p. 476-480
3. Arai T., et al. /Chem. Mater., 2008, v. 20, p. 1997-2003

EFFECT OF ORGANIC CARBON AND NITROGEN SOURCES ON THE BACTERIOCIN PRODUCTION BY LACTOBACILLUS DELBRUECKII SPP. LACTIS STRAIN A7

S.G.GULAHMADOV, V.SH.NAZARLI, A.A.KULIEV[1]

Baku State University, Departament of Biochemistry and Biotechnology, Faculty of Biology, Baku, Azerbaijan.
(Received 5 May, 2015)

The aim of this work was to investigate the effect of carbon and nitrogen sources on the maximum activity of bacteriocin production by *Lactobacillus delbrueckii* spp. *Lactis* A7. The bacteriocin was produced at maximum activity in M17 broth supplemented with 0.5% lactose (M17L). Moreover, carbon and nitrogen sources significantly influenced the production of bacteriocin. The bacteriocin yield was at least 3,6-fold higher in M17 broth supplemented with lactose compared to other carbon sources. The optimal organic nitrogen source for bacteriocin production was yeast extract (3%). This optimization of bacteriocin production by modification of environmental growth conditions will greatly benefit efficient commercial application.

1. INTRODUCTION

Lactic acid bacteria (LAB) have a wide range of technological properties and are often used for the manufacture of various fermented foods [2, 5, 7, 12]. These bacteria currently play a major role in the production of fermented milk products due to proteolysis, lipolysis and citrate splitting, hence adding a unique flavor and aroma to these products [1, 12, 13]. They also play the role of protective agents against various pathogens, including genus *Listeria*, a known microbe, which present in meat and dairy products. This is due to their ability to release a number of metabolites with antimicrobial properties. One of these antimicrobial metabolites is bacteriocins, molecules of peptide nature synthesized on ribosomes [2, 6, 19].

The species of the genus *Lactobacillus* have long been used as a starter culture for the manufacture of various types of fermented milk products. However, in the presence of virulent factors in their genome, they are associated with pathogenicity. Consequently, for bioprotect the products of fermentation, it is advisable to add neither the producer bacteria themselves but their bacteriocins as an additive [5, 14]. In such a case, it becomes necessary to optimize the bacteriocinogenesis process in order to obtain a sufficient amount of this antimicrobial substance. This process depends on many factors, which are usually a strain specific [8, 20].

Bacteriocinogenic strain *Lactobacillus delbrueckii spp. Lactis A7*, isolated from breast milk, has a broad spectrum of antimicrobial activity and some positive probiotic properties. Synthesis of bacteriocin of this strain occurred at an early stage of the exponential growth phase of the strain.

The highest bacteriocin titer was detected at the end of the exponential phase and at the initial stage of the stationary growth phase at a temperature of $+37^0$ C and the starting value of pH culture 6.5 [10].

Considering the above listed useful properties of the strain *Lactobacillus delbrueckii spp. Lactis A7*, in this work we studied the effect of organic sources of carbon and nitrogen on the production of its bacteriocin.

2. EXPERIMENTAL

The bacteriocin-producing strain used in this study *Lactobacillus delbrueckii* spp. *Lactis* A7 was isolated from breast milk [10]. *Lactobacillus bulgaricus* 340 was used as an indicator strain. The stock culture and indicator strain were maintained at –20°C in MRS broth (Difco) containing 25% (v/v) glycerol. *Lactobacillus bulgaricus* 340 was cultured at 37°C overnight. *Lactobacillus delbrueckii* spp. *Lactis* A7 culture was propagated twice in either MRS or M17 broth at 30°C for 16 h before use in experiments.

M17 broth [22] contains ascorbic acid (0.5 g/1), MgSO4 (0.25 g/1), disodium-β-glycerophosphate (19 g/1), tryptone (5 g/1), soytone (5 g/1), beef extract (5 g/1) and yeast extract (2.5 g/1). *Lactobacillus delbrueckii*

spp. *Lactis* A7 was cultured in M17 broth (Difco) supplemented with 0.5% lactose (M17L broth). M17L broth, 250 ml in 500 ml Erlenmeyer flasks were inoculated with 1.0% overnight cultures. The flasks were incubated without agitation at 30°C for 12 h. Initial pH of flask cultures was adjusted to pH 6.5. Samples of 5 ml were withdrawn from the flasks aseptically at 2 h intervals, and tested for bacterial cell density, pH and bacteriocin activities. All experiments were performed in triplicate.

Bacteriocin activity was determined by a dilution-method [8]. After centrifugation (10,000 g) of samples at 4°C for 15 min, the supernatant was filter-sterilized (0.22 μm, Millex-GV filter, Millipore). Bacteriocin was detected as follows: serial two-fold dilutions of the supernatant were made in 125 μl volumes of TSB in a 96-well microplate. Each well was inoculated with 50 μl of a 100-fold diluted overnight culture of the indicator strain. The microplate was then incubated at 37°C for 16 h. Bacteriocin activity was expressed as arbitrary unit per ml (AU/ml) and calculated from the formula $(1,000/125)\times(1/HD)$, where HD is the highest dilution that allowed no growth of the indicator strain. Bacterial growth was determined by measuring optical density (OD) at 600 nm using a spectrophotometer.

To examine the effect of carbon sources on bacteriocin production by *Lactobacillus delbrueckii* spp. *Lactis* A7, different carbon sources (galactose, glucose, D-fructose, maltose, mannitol, lactose, rybose, sucrose or sellobiose) were added to M17 broth to 0.5% and incubations were carried out at 37°C for 16 h. M17L medium without carbon source was used as a control. To determine the influence of different nitrogen sources on bacteriocin production, different nitrogen sources (beef extract, yeast extract, tryptone, peptone, casein or soytone) were added to basal medium at 1.0% level and incubations were carried out at 37°C for 16 h. The basal medium (lactose, 5 g/1; ascorbic acid, 0.5 g/1; MgSO4, 0.25 g/1; disodium-β-glycerophosphate, 19 g/1) was based on M17L medium, in which all nitrogen sources (soytone, 5 g/1; beef extract, 5 g/1; yeast extract, 2.5 g/1; tryptone, 5 g/1) were eliminated. Bacteriocin production was also investigated with different concentrations of yeast extract at 37°C for 16 h.

Various concentrations (0.5, 1, 2, 2,5, 3, 3,5, 4, 5%) of yeast extract were added to basal medium. M17L medium was used as a control. Bacteriocin production (AU/ml) and bacterial growth were detected as described above.

3. RESULTS AND DISCUSSION

In order to determine the role of carbon sources in this process, we cultivated the producer strain in M17 medium, which was added with 0.5% concentration. As the organic sources of carbon, 9 different carbohydrates were tested - galactose, glucose, fructose, lactose, maltose, mannitol, ribose, sucrose and cellobiose. The results of these experiments are shown in Fig. 1. It can be seen from this figure that galactose, glucose, lactose and cellobiose were suitable sources of carbon for the growth of *Lactobacillus delbrueckii* spp. *Lactis* A7.

However, in the presence of lactose, the bacteriocin titer was 3.6 times higher than with the remaining three carbohydrates and was 1800 AU/ml. On the other hand, the weakest growth of the strain was found in the medium with maltose and ribose. The last carbon source also gave the smallest bacterioocin titer. Similar results were obtained for the production of bacteriocin AA11 and nisin, synthesized by *L. acidophilus* AA11 and *L. lactis* subsp. *lactis* A164, respectively [2, 7]. However, for synthesis and secretion of bacteriocin of the strain *Lactococcus lactis*, the most suitable source of carbon was xylose [1]. In other sources, it was reported that glucose and not lactose were the best source of carbon for the synthesis of bacteriocins *L. plantarum* YJG, *L. brevis* OG1 [9] and another probiotic strains of the *Lactobacillus* genera [7, 9, 22].

As described above, carbon sources were added to the culture medium in an amount of 0.5%.

Next, we investigated the effect of 1, 3, 5, 6, 7 and 9 g / l lactose concentrations in the M17 medium on the synthesis of bacteriocin by *Lactobacillus delbrueckii* spp. *Lactis* A7. The results of these experiments were summarized in Fig. 2. It follows from this figure, that in the absence of lactose in the medium, bacteriocin synthesis did not occur.

However, the addition of this carbohydrate at a concentration of 1 g / l (0.1%) led to the appearance of bacteriocin activity in a medium with a titer of 400 AU/ml. As the concentration of lactose in the medium increased, the activity of bacteriocin also increased. The titer of bacteriocin in the presence of 0.3% lactose was 900 AU/ml, 0.5% lactose - 1800 AU/ml, 0.6% - 3600 AU/ml, and at an effector concentration of 0.7% bacteriocin titer exceeded the starting value 18 times and reached the level of 7200 AU/ml. Further increase in lactose concentration did not affect the level of bacteriocin titer.
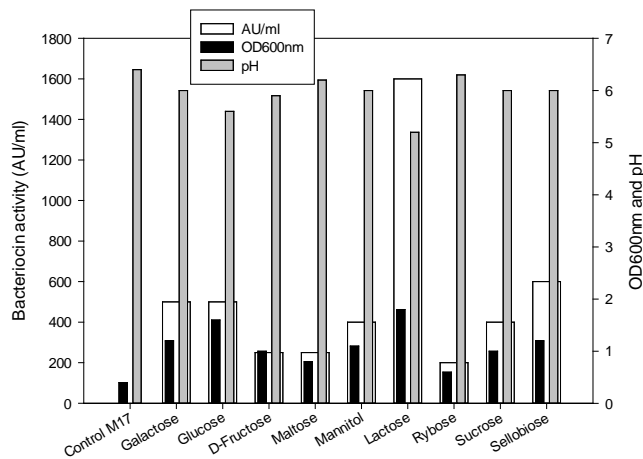
Figure 1. The effect of carbon sources on growth, pH of medium and synthesis of bacteriocin by *Lactobacillus delbrueckii* spp. *Lactis* A7 at + 37⁰C. M17 medium without a carbon source was taken as a control variant

Thus, the best source of organic carbon for the synthesis of bacteriocin strain *Lactobacillus delbrueckii* spp. *Lactis* A7 was lactose. The highest activity of bacteriocin was detected at a concentration of 0.7 g / l.

Further, we conducted similar experiments to study the effect of organic sources of nitrogen in the medium. For this purpose, we cultivated *Lactobacillus delbrueckii* spp. *Lactis* A7 in M17 medium to which nitrogen sources were added at a concentration of 1%. As an organic source of nitrogen, 5 different variants were tested - yeast extract, meat extract, casein, tryptone and peptone.

+37⁰C. M17 medium without lactose was taken as a control variant

The results of these experiments are shown in Fig. 3, from which it can be seen that the highest bacteriocin titer (1400 AU/ml) was detected in M17 medium in which yeast extract was added: the activity was almost three times greater than that found in the presence of tryptone. In a medium with this nitrogen source, the growth of the strain was quite high and the bacteriocin titer was 500 AU/ml.

This indicates that to obtain a sufficient amount of bacteriocin *Lactobacillus delbrueckii* spp. *Lactis* A7, yeast extract can be used as the sole source of nitrogen in the M17 medium. The result obtained is of great economic importance, since it reduces the expenditure of surplus funds for obtaining bacteriocin in an equivalent amount.

The weakest growth of the strain was found in the medium with casein and meat extract. In the presence of these sources, bacteriocin activity was in trace amount. Similar results were obtained for the production of bacteriocins AA11, OG1 and nisin of the *L. acidophilus* AA11, *L. brevis* OG1 and *L. lactis* subsp. *lactis* A164 strains, respectively [2, 7, 9, 15]. However, peptone was the most suitable source of nitrogen for the synthesis of the maximum bacteriocin titer by *Lactococcus lactis* strain [16].

Further, the dependence of the bacteriocin activity of the strain *Lactobacillus delbrueckii* spp. *Lactis* A7 from different concentrations of yeast extract.

Figure. 2. The effect of different concentrations of lactose on growth, pH of medium and synthesis of bacteriocin by *Lactobacillus delbrueckii* spp. *Lactis* A7 at
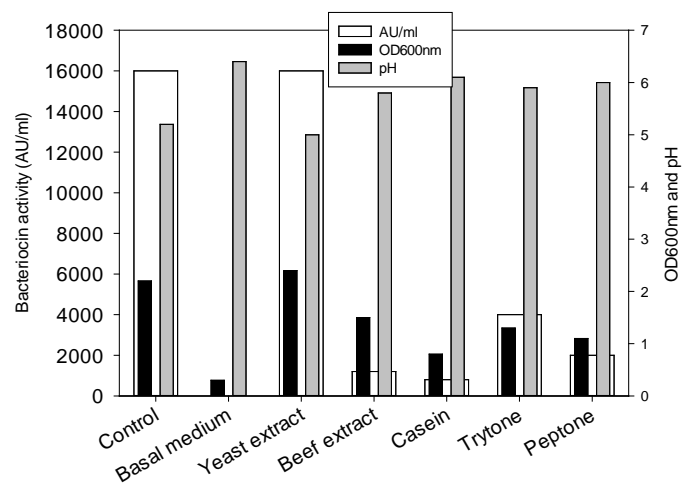
Figure 3. The effect of nitrogen sources on growth, pH of medium and synthesis of bacteriocin by *Lactobacillus delbrueckii* spp. *Lactis* A7 at + 37⁰C. The base medium is prepared on the basis of M17 medium without nitrogen sources

As already noted, nitrogen sources were added to the 1% cultivation medium. For this purpose, variants were used with 0.5%, 1%, 2%, 2.5%, 3%, 3.5%, 4% and 5% yeast extract in the M17 medium. The results of these experiments were summarized in Fig. 4.

It follows from this figure that in the absence of an effector in the medium, bacteriocin synthesis did not occur. However, the addition of this extract to a concentration of 0.5% led to the appearance of bacteriocin activity in a medium with a titer of 700 AU/ml. As the yeast extract concentration increased, bacteriocin activity also increased in the medium.

However, the stimulating effect of the nitrogen source continued until its concentration in the medium was equal to 3%. Titer of bacteriocin in the presence of 1% yeast extract was 1400 AU/ml, 2% - 1800 AU/ml, 2.5% - 3400 AU/ml. Effector concentration Increasing to 3% led to the fact that the bacteriocin titer exceeded the starting value by more than 6 times and reached the level of 4400 AU/ml. Further increase in yeast extract concentration did not affect the level of bacteriocin titer. Similar indicators for the strain of *L. acidophilus* AA11 were 4%. The stimulating effect of the yeast extract may be due to the fact that, in comparison with the products of hydrolysis of other organic nitrogen sources, this extract has in its composition a richer assortment of free amino acid residues and short oligopeptides consisting of two or three amino acid residues, as well as many growth factors [2, 9, 17].
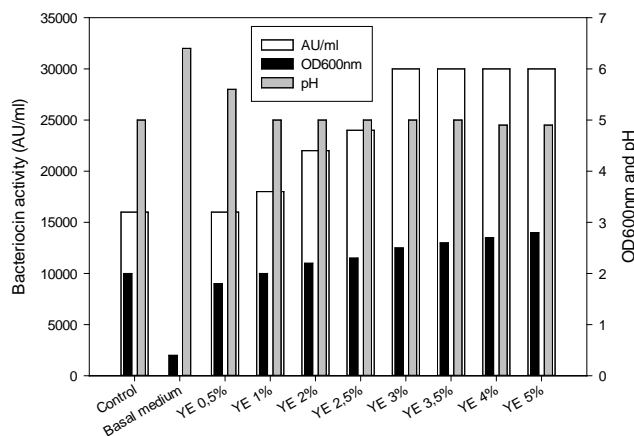
Figure 4. Effect of different concentrations of yeast extract on growth, pH of medium and synthesis of bacteriocin by *Lactobacillus delbrueckii* spp. *Lactis* A7 at + 37^{0}C. M17 medium without yeast extract was adopted as a control variant.

Thus, the best source of organic carbon for the synthesis of bacteriocin strain *Lactobacillus delbrueckii* spp. *Lactis* A7 was lactose (0.7 g/l), and source of nitrogen was yeast extract. The highest activity of bacteriocin was detected at a concentration of 3%. The results obtained in this work suggest that factors of the culture medium, including carbon and nitrogen sources, have a significant influence on the bacteriocin biosynthesis process. These data can be very useful for the more economical production of these natural biosecurity in developing methods.

4. CONCLUSION

The best source of organic carbon for bacteriocin synthesis by *Lactobacillus delbrueckii* spp. *Lactis* A7 was lactose (0.7 g/l), and source of nitrogen was yeast extract. The highest bacteriocin activity was detected at a concentration of 3%.

5. REFERENCES

1. Aasen I., Moretro T., et al. /Appl Microbiol Biotechnol., 2000, v.53, pp.159–166
2. Abo-Amer A. E. / Acta Microbiol Immunol Hung, 2007, v. 54, pp.107–119
3. Barada N. / J. Dairy Sci., 1991, v.74, pp.409-413
4. Benkerroum, N., Ghoati Y., Ghalfi H. / Biotechnol, 2007, v.6, pp.481-488
5. Brandtzaeg P. / Nestle Nutr Workshop Ser Pediatr Program., 2009, v.64, pp.23–38
6. Chang Y., Kim J., et al. / Antonie van Leeuwenhoek, 2001, v.80, pp.193–199
7. Cheigh C., Choi H., et al. / J Biotechnol, 2002, v. 95, pp.225-235
8. Daba H, Pandian S, et al. / Appl Environ Microbiol, 1991. V.57, pp. 3450–3455
9. Elsayed A. Characterization and Genetic Improvement of *Lactobacilli* for Application in Probiotic Products. PhD thesis, University of Kiel, Germany, 2007
10. Gulahmdov S.G., Abdullaeva N. A., et al./ Advances in Biology & Earth Sciences. 2017, Vol. 2, No.2. pp. 186-191
11. Hoppu U, Isolauri E, et al. / Eur J Nutr, 2012, v. 51, pp. 211–219.
12. Hummel A., Hertel C., et al./ Appl. Environ. Microbiol., 2007, v.73(3), pp.730-739
13. Kanatani K., Oshimura M., Sano K. / J. App. Envir. Microbiol., 1995, v.61, pp.1061–1067

14. Khavkin A.I. /Moscow Research Institute of Pediatrics and Pediatric Surgery. Particular issues of pediatrics, 2007, v. 9, No. 1, art. 4-24

15. Klaenhammer, T., Kullen, M. / Int. J. Food Microbiol., 1999, v.50, pp.45–57

16. Kos B, Suskovic J, Beganovic J, et al. / World J Microbiol Biotechnol., 2008, v.24, pp.699–707

17. Lauková, A., Czikková, S. / Journal of Applied Microbiology, 1999, v.87, pp.182–186

18. Ludtke S., He K., Heller W. et al. / Biochemistry, 1996, v.35, pp.13723–13728

19. Martín R., Olivares M., et al./ Journal of Human Lactation., 2005, v.21(1), pp.8-17

20. McAuliffe O., Cano R., et al. / Appl. and Environ. Microbiol., 2005, v.71(8), pp.4925–4929

21. Saxelin M., Tynkkynen S., et al./ Curr. Opin. Biotechnol., 2005, v.16, pp.204–211

22. Terzaghi B.E., Sandine W.E. / Appl Microbiol., 1975, v. 29. pp.807–813

Journal of LDS